


# An alternative Vorticity based Adaptive Mesh Refinement (V-AMR) technique for tip vortex cavitation modelling of propellers using CFD methods

Savas Sezen  and Mehmet Atlar

Naval Architecture, Ocean & Marine Engineering, University of Strathclyde, Glasgow, UK

## ABSTRACT

This study focuses on the investigation of cavitating flow around the benchmark INSEAN E779A model propeller with the main aim of further improving the computational efficiency of the tip vortex cavitation (TVC) modelling by using a commercial CFD solver. Also, the effects of various key computational parameters including, numerical modelling, grid size, timestep, water quality and boundary layer resolution, on the TVC formation and its extension in the propeller slipstream are investigated systematically.

The numerical simulations are conducted in uniform and open water conditions using RANS, DES and LES solvers implemented in the commercial CFD code, Start CCM+. In order to achieve the aim of the study, an alternative and new Vorticity-based Adaptive Mesh Refinement (V-AMR) technique is introduced for enhanced modelling of the TVC on the blades and downstream. For the CFD modelling of cavitation, the Schneer Sauer cavitation model based on the reduced Rayleigh Plesset equation is used for the sheet, tip and hub vortex cavitation. The hydrodynamic results and cavity patterns are validated with the experimental data. The results show that the application of the V-AMR technique further improves the representation of the TVC with minimal increase in computational cost. However, the eddy viscosity at the propeller blade tips increases with applying the V-AMR technique using the RANS solver due to its inherent modelling errors for the solution of the flow inside the tip vortex. This consequently results in an insufficient extension of TVC in the propeller slipstream compared to the predictions by the DES and LES based numerical solvers. Also, the evolution of the TVC is found to be sensitive to the boundary layer resolution when the standard RANS solver is used. The study will help to widen further applications of the CFD methods involving TVC, particularly for propeller induced underwater noise prediction and analysis.

## ARTICLE HISTORY

Received 19 November 2020  
Accepted 2 May 2021

## KEYWORDS

Adaptive Mesh Refinement (AMR); Tip Vortex Cavitation (TVC); RANS; DES; LES; E779A

## 1. Introduction

Propeller cavitation is of great interest for ships due to the resulting powering performance degradation, blade erosion, hull, and shaft vibrations, as well as the underwater radiated noise (URN). The type, extension and dynamics of the propeller cavitation are dependent on the propeller geometry, its operating condition, water quality as well as the wake flow of the ship's hull in front of the propeller. Amongst the different propeller cavitation types, such as bubble, sheet, cloud, and vortex, the ship propellers commonly operate in conditions where the sheet and tip vortex cavitation are observed in combination (Bosschers 2018).

The numerical studies related to cavitation have mainly focused on sheet cavitation, which is deemed to be more harmful than vortex cavitation. In this regard, the potential flow-based solvers (i.e. lifting surface and panel methods) are generally used in the propellers' early design stage to account for the sheet cavitation and its effects on the propeller hydrodynamic performance (e.g. Fine and Kinnas 1993; Lee

and Kinnas 2004). However, the potential flow solvers may have some drawbacks for accurate predicting the cavitation dynamics compared to viscous flow solvers. The reason being, they ignore the effects of viscosity even though the empirical method is used to add the viscous drag in the calculations. Including the viscosity in the computations enables to predict the shedding of the sheet and tip vortex cavities in a more accurate way (Sipilä 2012). Therefore, different viscous flow solvers, e.g. RANS (Reynolds-averaged Navier Stokes), DES (Detached Eddy Simulation) and LES (Large Eddy Simulation), are alternative ways to model the cavitating flow for marine propellers (e.g. Bensow and Bark 2010; Viitanen and Siikonen 2017; Gaggero et al. 2014).

The numerical prediction of cavitation phenomena is complicated compared to non-cavitating conditions, not only because of the multi-phase nature of cavitation. But also due to the strong interactions between the turbulent flow and cavitation dynamics, and selection of different simulation techniques (e.g. RANS, DES, LES) and numerical modelling

**CONTACT** Savas Sezen  savas.sezen@strath.ac.uk

parameters used (e.g. timestep, grid resolution, water quality, etc.) (Lloyd et al. 2017). One of the main difficulties in the cavitating propeller flow computations is to model the tip vortex cavitation (TVC), which is related to cavitation inception speed (CIS), and usually occurs as the first type of cavitation on well-designed propellers. The anisotropic turbulence and higher velocity gradients in all directions inside the vortex core make the evaluation of the tip vortex flow difficult. The prediction of the strength and size of a tip vortex, which is driven by both viscous diffusion and vortex lines, along its trajectory is a complex flow phenomenon. This is further complicated by the complex physical dynamics between the vortex structures and different pressure fields created within the surrounding and inside the vortex core (Hunt et al. 1988; Asnaghi 2018; Asnaghi et al. 2020). Hence, a realistic solution of the flow inside the vortex core enables to model the TVC in the propeller slipstream under cavitating conditions. TVC is also one of the important sources of a URN, especially in the presence of the bubble collapse or bursting phenomenon in the non-uniform wake (Konno et al. 2002). It consequently influences the overall noise spectrum and hull-pressure fluctuations. Thus, physical understanding and numerical modelling of the TVC is still an important topic in propeller hydrodynamics.

In recent years, several studies have been conducted to investigate the tip vortex flow under non-cavitating conditions using experimental and numerical methods in the literature (e.g. Felli et al. 2011; Muscari et al. 2013; Qiu et al. 2013; Guilmineau et al. 2015). As well as these investigations, the inception of TVC has been studied with hydrofoil geometries and marine propellers using different simulation techniques and hence numerical solvers. Hsiao and Chahine 2008 performed a numerical study to examine TVC inception of marine propellers. RANS and DNSS (Direct Navier Stokes Simulations) methods were utilised together to increase the accuracy of the RANS solution for the tip vortex flow. DNSS was performed in a reduced domain by taking the boundary conditions from the initial RANS solution. The results showed that the RANS solution was inadequate to resolve the continuous roll-up process, except the initial roll-up, due to the averaging nature and insufficient turbulence modelling. Gaggero et al. 2014 investigated the inception of tip vortex and tip leakage vortex cavitation using a RANS solver with Schneer-Sauer cavitation model for conventional and two ducted propellers. Their results showed that the RANS method could be reliably used as a primary design tool for engineering purposes to predict the inception of TVC. Also, the tip vortex flow solution inside the vortex core was found to be more sensitive to the grid resolution than the cavitation model parameters (i.e. nuclei density and diameter). Gosda et al., (2018) studied the Reynolds

number scale effects on propeller tip vortex cavitation and propeller-induced hull-pressure fluctuations using a two-dimensional vortex model. The interaction between the circumferential velocity and the cavity in the vortex was captured with the applied method. Asnaghi et al. 2020 performed a comprehensive numerical study for the investigation of tip vortex flow under cavitating and wetted flow (i.e. non-cavitating) conditions for an elliptical foil. The grid resolution requirements were assessed for the solution of the flow inside the vortex core using LES. The numerical results showed that it is important to adopt sufficient cells for the accurate solution of tip vortex flow.

As stated in the above review of some relevant studies, the solution of the tip vortex requires an accurate calculation of the minimum pressure inside the vortex. Thus, the realistic solution of the tip vortex flow is strongly dependent on the grid resolution inside the vortex and numerical modelling techniques. In the numerical computations, priority local mesh refinements (i.e. tube and spiral) are generally adopted at the propeller blade tips to decrease the numerical diffusion for the formation of tip vortex; hence, TVC (e.g. Usta and Korkut 2018; Zhu 2019). However, these approaches have not been sufficiently successful, and they are computationally expensive due to the excessive amount of cells used to model the TVC in the propeller slipstream. Also, it is not practical to adopt high-resolution grids in the entire propeller slipstream as the computational cost would be escalated. Therefore, the grid refinement should be implemented as local as possible at the tip vortex regions to decrease the computational cost and predict the minimum pressure inside the vortex core. This can be achieved using the Adaptive Mesh Refinement (AMR) technique, which has been implemented relatively recently in the hydrodynamic field for isolated propeller cases and complete models (i.e. propeller together with hull) both in the model and full-scales. In the studies of Wackers et al. 2010 and Queutey et al. 2012, the flow around the hull and propeller was solved using an in-house unsteady RANS solver, which was integrated with AMR. The AMR technique was found to be successful for the solution of the free surface and vorticity field. Windt and Bosschers 2015 performed AGR (Adaptive Grid Refinement) technique and local mesh refinement to investigate the minimum pressure in the tip vortex core for a rectangular wing and single propeller blade in open water conditions. The computations showed that both methods improved the accuracy of the solution, but the total number of cells in AGR were found three times lower than the local mesh refinement. Yvin and Muller 2016 studied the assessment of the tip vortex cavitation inception without using the cavitation model for a marine propeller. In the

computational model, an automated mesh refinement technique was used to evaluate the minimum pressure inside the vortex core using the RANS based EASM (Explicit Algebraic Stress Model). Lloyd et al. 2017 employed the local mesh refinement and AGR technique using RANS and DES methods by modelling a single blade for INSEAN E779A propeller, which is also used in the present study. The results showed that the details of the vortex roll-up in the AGR technique were predicted better than using local mesh refinements. Also, the different types of AMR techniques have been recently implemented by Shin and Andersen 2018; Yilmaz et al. 2019 and Krasilnikov 2019 to model TVC.

Although there have been recent numerical studies to model the TVC in the propeller slipstream, the TVC phenomenon, the computational cost of the current methods are still high; thus, a single blade is usually modelled (e.g. Lloyd et al. 2017). There are also very recent studies for all blades TVC simulations using attractive AMR techniques (e.g. Yilmaz et al. 2019). However, these studies used extensive mesh numbers and associated computational resources that would limit to expand these techniques for modelling the cavitation induced radiated noise from the propellers both in model and full-scale, which is the main motivation and ultimate goal of the authors. This study, therefore, investigates more computationally efficient TVC modelling emanating from all propeller blades to provide a basis for the cavitation induced underwater radiated noise modelling. Also, to the best of the authors' knowledge, the influence of the different simulation methods (e.g. RANS, DES, LES) and that of some key computational prediction parameters such as grid resolution, timestep and water quality parameters (e.g. nuclei number and nuclei density) on the TVC have not been comprehensively investigated. Therefore, this study aims to make a contribution to this field by introducing an alternative Vorticity-based AMR, the V-AMR technique, for a more accurate representation of the TVC in the propeller slipstream and exploring the effects of the different simulation methods and other key modelling parameters using a commercial CFD solver (i.e. Star CCM+ 14.06).

In this study, the cavitating flow around the benchmark INSEAN E779A propeller was investigated in uniform and open water conditions using RANS, DES and LES solvers. The Schnerr-Sauer cavitation model based on the reduced Rayleigh Plesset equation was coupled with the V-AMR technique to model the sheet and tip vortex cavitation. The predicted results and cavity patterns were validated with the experimental data, and the results were discussed with an emphasis on the efficiency of V-AMR. The pros and cons of the RANS, DES and LES solvers were investigated in a comparative manner in modelling the sheet,

hub and tip vortex cavitation. Finally, the effects of some key parameters in cavitating modelling and simulation as well as on the evolution of TVC were examined systematically.

Within the above framework, following this introductory Section 1, the paper presents the details of the theoretical model for the propeller flow in Section 2. The numerical implementation of the CFD method and including the propeller geometry, computational domain & boundary conditions and V-AMR procedure, are presented in Section 3. The numerical results and discussions are given in Section 4. Finally, the conclusions drawn from the study are presented in Section 5.

## 2. Theoretical background

The simulations were conducted by using the Star CCM+ commercial solver under cavitating conditions. Cavitation is a phase change and assumed to occur when the static pressure at a particular location within the liquid becomes equal or smaller than the saturation vapour pressure, also depending on the water quality. Cavitation bubbles are assumed to consist of cavitation nuclei which are tiny bubbles filled with vapour or gas or a combination of them. The number of small nuclei is higher than those of larger nuclei in the fluid due to the stable nature of the small bubbles under their higher surface tension (Sipilä 2012). In this study, the Schnerr-Sauer cavitation model based on the reduced Rayleigh Plesset equation was used to model sheet and tip vortex cavitation as a default modelling tool (Star CCM+ 14.06 2019). In this model, seeds are assumed to be spherical and uniformly distributed in the liquid, and all seeds initially have the same radius. The Volume of Fluid (VOF) method, which was first introduced by Hirt and Nichols 1981, was used to describe the phase transition of liquid into vapour or vice versa. Detailed information about the VOF and cavitation model can be found in Star CCM+ 14.06 and Schnerr and Sauer 2001, respectively.

In the numerical simulations, the three different simulation methods, RANS, DES and LES, and the associated solvers were used to solve the flow around the cavitating propeller. The RANS solver is based on the solution of the time-averaged equations in the fluid domain, whereas LES is based on filtered differential equations. DES is a hybrid method by combining the RANS in the boundary layer and LES in the free field region. The improved formulation of DES (i.e. Delayed DES) was used in this study. The  $k-\omega$  SST turbulence model was selected both for the RANS and DDES solvers. Additionally, the WALE (Wall-Adapting Local-Eddy viscosity) subgrid-scale model was used to close the filtered Navier-Stokes equations for the LES. Also, the large scales of the

turbulence are directly resolved everywhere in the flow domain in the LES while the small scales are modelled. Despite its several limitations, the RANS method is still used for many engineering problems due to its lower computational cost compared to scale resolving simulations (i.e. DES and LES), particularly in the design stage. The detailed information about the solvers can be found in Spalart et al. 2006 and Star CCM+ 14.06 (2019).

In the above described three different solvers, the segregated flow model was used with SIMPLE type algorithm between the continuity and momentum equations. The second-order implicit unsteady scheme was employed for the time discretisation. As well as this, the convection term was discretised using the second-order scheme in the RANS and DES applications, whereas its discretisation was provided with the bounded central scheme for the LES. The propeller rotational motion was modelled using the RBM (Rigid Body Motion) approach in an unsteady manner, while the MRF (Moving Reference Frame) approach was also used as an initial solution in a steady manner for the unsteady simulations. The simulations were initially started without a cavitation model using the MRF approach to avoid any numerical problems due to the cavitation. The inner iteration was set to 7 for all models.

### 3. Numerical model

#### 3.1. Test case

The benchmark INSEAN E779A model propeller was selected in this study. The cavitating flow around this model propeller was compared with the numerical solutions conducted by different facilities in the scope of the Rome 2008 Workshop in uniform flow under non-cavitating and cavitating conditions (Salvatore et al. 2009). The non-cavitating results were found to be

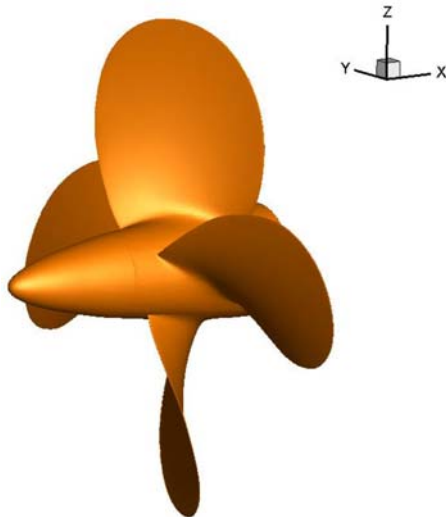


**Figure 1.** 3D view of the INSEAN E779A model propeller.

**Table 1.** The main particulars of the propeller.

Number of Blades	$Z$	4
Diameter (m)	$D$	0.227
Pitch Ratio ( $P/D$ )	$P/D$	1.1
Expanded Area Ratio	$(A_E/A_0)$	0.689

in good agreement with each other, whereas some discrepancies were observed for the cavitating flow case. Also, the TVC could not be predicted successfully by using different flow solvers. Thus, this propeller was deemed to be a suitable test case to show the capabilities of the V-AMR technique. Figure 1 and Table 1 show the 3D view and main particulars of the test propeller, respectively.

The numerical simulations were performed both in the presence of sheet, hub and tip vortex cavitation and only including the sheet and hub vortex cavitation cases. In this way, the capabilities of the V-AMR technique would be proven at different levels. Table 2 summarises the properties of the test case.

In presenting the test results, various non-dimensional coefficients were used to present the propeller performance, and these are described in the following.

The cavitation number is defined with respect to the propeller rotational rate in Equation (1).

$$\sigma = \frac{P_0 - P_V}{\frac{1}{2}\rho(nD)^2} \quad (1)$$

where  $P_0$  is the static pressure; Pa,  $P_V$  is the vapour pressure; Pa,  $\rho$  is the density of the fluid;  $\text{kg/m}^3$ ,  $n$  is the propeller rotational rate; rps,  $D$  is the propeller diameter; m.

The advance ratio ( $J$ ) is defined in Equation (2);

$$J = \frac{V_A}{nD} \quad (2)$$

where,  $V_A$  is the average flow velocity at the propeller plane; m/s.

The thrust ( $K_T$ ), torque ( $K_Q$ ) coefficients and efficiency ( $\eta_0$ ) are defined in the following Equations, respectively.

$$K_T = \frac{T}{\rho n^2 D^4} \quad (3)$$

$$K_Q = \frac{Q}{\rho n^2 D^5} \quad (4)$$

$$\eta_0 = \frac{J K_T}{2\pi K_Q} \quad (5)$$

**Table 2.** Test case description.

Parameter	Symbol and Unit	Value
Advance ratio	$J$ (-)	0.71
Rotation Rate	$n$ (rps)	36
Inflow averaged velocity	$V_A$ (m/s)	5.8
Cavitation number	$\sigma$ (-)	1.763
Vapour pressure	$P_V$ (Pa)	2337

Here,  $T$  is thrust;  $N$  and  $Q$  is the torque of the propeller; N.m.

### 3.2. Computational domain and boundary conditions

Figure 2 shows the computational domain used in the numerical calculations. The domain was extended by 3D and 7D at the upstream and downstream of the propeller centre, respectively, whereas the radius of the domain was set to 4D. The red surface of the domain is the velocity inlet, whereas the green surface is the pressure outlet. The remaining surfaces of the domain were defined as symmetry planes. In addition, the propeller blades and hub were identified as a wall with the no-slip condition to satisfy the kinematic boundary condition. The transition between the rotating and static regions was provided with the sliding interfaces.

### 3.3. Grid structure and Adaptive Mesh refinement (AMR) technique

The implementation of a suitable grid structure is important for the accuracy of the numerical solution. Thus, the grid should be as adequate as possible to solve the flow around cavitating propellers but in an efficient manner to avoid impracticalities. In particular, the solution of the tip vortex is more dependent on the grid resolution inside the vortex, and it requires high-resolution grids in all directions. However, inevitably, the application of high-resolution grids in the entire propeller slipstream would increase the total cell number in the numerical calculations, which results in an increased computational cost. Thus, AMR becomes appealing as it can decrease the computational cost considerably while still accurately predicting the area of interest.

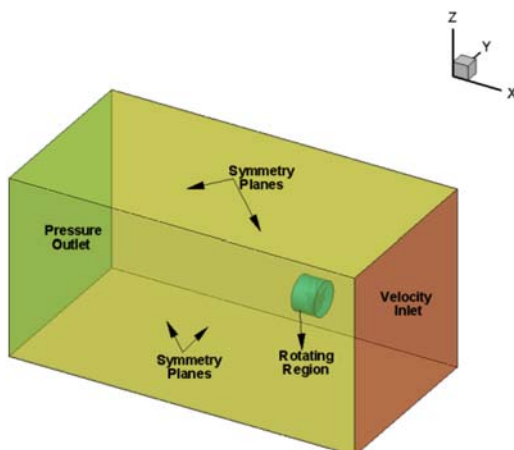


Figure 2. Representation of computational domain.

AMR is a dynamic mesh technique, and it refines or coarsens the cells in the specified regions of the computational domain according to the adaptive mesh criteria. The solution quantities are automatically interpolated to the new adapted mesh locations. One of the challenges in the AMR technique is the selection of an appropriate refinement criterion. The refinement criterion can be selected either as a scalar quantity (e.g. pressure) or as a gradient (e.g. vorticity) quantity to create the cells in the tip vortex trajectory. As stated in the study of Yvin and Muller 2016, the shape of the pressure field in the transversal direction looks like a Gaussian function; thus, it is difficult to conclude whether the location of the minimum pressure inside the vortex is in the centre or not. For this reason, it was suggested that the refinement criterion should not be chosen value of pressure itself (Yvin and Muller 2016). Hence, the vorticity based  $Q$  criterion was selected as the refinement criterion for the AMR application in this study. The  $Q$  criterion can be defined with the following Equation;

$$Q = 1/2[(|\Omega|^2 - |S|^2)] \quad (6)$$

where  $S$  denotes the strain rate tensor and  $\Omega$  is the angular rotation rate tensor (or vorticity tensor). According to the magnitude of  $Q$  the criterion, the dominant parameter in the flow field can be determined. When the value of  $Q$  the criterion is positive, the flow field is dominated by the vorticity, whereas the strain rate dominates the flow field when the  $Q$  criterion value is negative (Star CCM+ 14.06).

As well as the refinement criterion, it is also important to select the suitable cell size for the accurate solution of flow inside the vortex. In this regard, Asnaghi 2018; Asnaghi et al. 2020 performed a comprehensive numerical study to investigate the cell numbers per vortex radius for the accurate solution of the tip vortex flow for an elliptical foil. Kuiper 1981 also conducted a series of experimental tests using different model scale propellers for investigating the bubble, sheet and tip vortex cavitations. Kuiper 1981 investigated the relationship between cavitation index ( $\sigma$ ) and core radius ( $a_c$ ). According to his experimental results, the core radius was measured around 0.25 mm at the cavitation inception for the model scale propellers. Hence, based on the analysis of these investigations (i.e. Kuiper 1981; Asnaghi 2018; Asnaghi et al. 2020), the vortex's cell size was set to be changed from 0.2 mm to 0.3 mm to detect the influence on TVC.

The proposed V-AMR technique involves two main steps. Once the flow field converges using the initial mesh (i.e. without AMR), the tip vortex areas can be visualised using the threshold value of  $Q$ -criterion (see Figure 3A). In this study, the threshold value of the  $Q$ -criterion was selected as  $Q = 400.000 \text{ 1/s}^2$  at the 1st stage to allow for sufficient

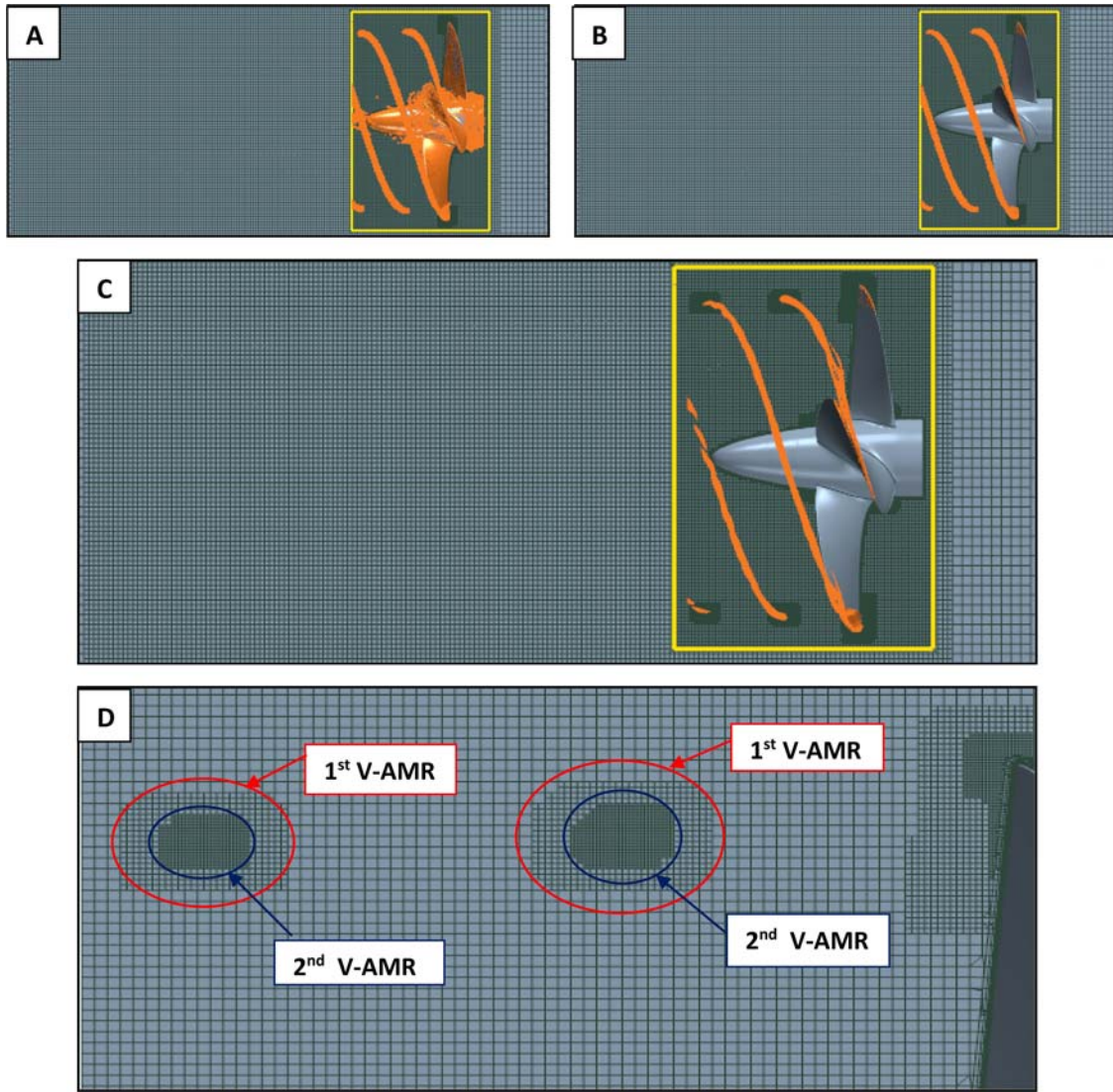


**Figure 3.** Refinement regions with V-AMR technique.

extension of the helical structure to the downstream of the rotating region boundary using the LES method. As can be seen in [Figure 3A](#), the helical structure of the tip vortex shows the regions where the magnitude of the  $Q$  criterion is higher than the selected threshold value (i.e.  $Q = 400.000 \frac{1}{s^2}$ ). It is also important to note that the determined refinement area with the threshold value of  $Q$  criterion shows the cells around the hub, which is not of interest. Hence, the additional user-based field functions were also imposed on the V-AMR solution algorithm to avoid the generation of the redundant cells, with the sole refinement located in the tip vortex trajectory (see [Figure 3B](#)). When the field of interest was determined, the refinement table was generated in all directions with the user-based field functions. At the 1st stage of the V-AMR procedure, the trajectory of the tip vortex was determined using relatively coarse grids. Following the 1st stage of the V-AMR (i.e. after two or three propeller revolutions), the 2<sup>nd</sup> stage of the V-AMR procedure was

implemented with the new threshold value of  $Q$  criterion ( $Q = 5.000.000 \frac{1}{s^2}$ ) in our case, (see [Figure 3C](#)). The advantage of this two-stage application of the V-AMR procedure is to decrease the total element count in the numerical solver and hence, the computational cost. The reason being, the actual tip vortex radius is small when compared to the helical structure of the tip vortex radius, which was determined in the 1st stage of V-AMR (see [Figure 3A](#)). If the V-AMR application were directly implemented with a smaller cell size (i.e. 2<sup>nd</sup> stages of V-AMR) without determining the tip vortex trajectory in the 1st stage of the V-AMR, the total element count would increase excessively. The adopted grid refinements can be seen in [Figure 3D](#) using the two stages of the V-AMR procedure. It is to be noted that the above procedure can be repeated three or four times to observe the TVC. However, from the authors' experience and some preliminary studies, it was found that any more than two stages do not

give considerable benefit in terms of the extension of the TVC in model scale for the application of the V-AMR procedure. Thus, two stages of V-AMR were implemented in this study. It is to be noted that the threshold value of the  $Q$  criterion is dependent on the operating condition. Hence, it should be set based on the visualisation of the tip vortex trajectory in the propeller slipstream.

In the numerical calculations, the unstructured grid was used to discretise the computational domain using the trimmer mesh approach in Star CCM+ 14.06 (2019). The same grid structure and refinement table were used for the RANS, DES and LES solvers. Later on, the effects of the grid on the extension of TVC were examined using different grid structures by the LES solver. The average  $y^+$  value on the propeller blades was kept under 1 for all solvers. In this way, the boundary layer was directly resolved without using the wall function approach. A flow chart for the developed V-AMR technique is also given in Figure 4 to summarise the algorithm used.

## 4. Numerical results

### 4.1. Influence of AMR on hydrodynamic field and cavitation

In this section, the results were presented with the initial mesh and further refinement of the mesh in order to see the effect of the V-AMR technique on

the hydrodynamic field around the propeller, hydrodynamic performance characteristics of the propeller, and TVC formation using the RANS, DES and LES solvers. The same grid structure, including the same cell size in the tip vortex region (i.e. 0.2 mm), the time-step (i.e.  $0.5^\circ$  of propeller rotation rate) and the default cavitation parameters (i.e. water quality) were used to concentrate on the comparison of the different simulations methods.

The effects of the V-AMR technique on the hydrodynamic field are compared with the two axial planes located at  $x/D=0.05$  and  $x/D=0.1$  in the propeller's slipstream using the three different solvers. Figures 5 and 6 shows the change in the non-dimensional pressure coefficient at the propeller blade tips where the tip vortex is more pronounced for  $x/D=0.05$  and  $x/D=0.1$ , respectively. As shown in Figures 5 and 6, the pressure inside the vortex core is lower than its surroundings, and it increases gradually outside of the vortex region. The overall distribution of the pressure field is found to be similar without the application of the V-AMR technique for different models at  $x/D=0.05$ . As further away in the propeller downstream, the low-pressure region is slightly more distinct using the LES solver without the V-AMR technique. However, the low-pressure region becomes more prominent with the RANS, DES and LES solvers applying the mesh refinement. Additionally, the low-pressure field is more stretched in the LES when compared to the RANS and DES at two different sections.

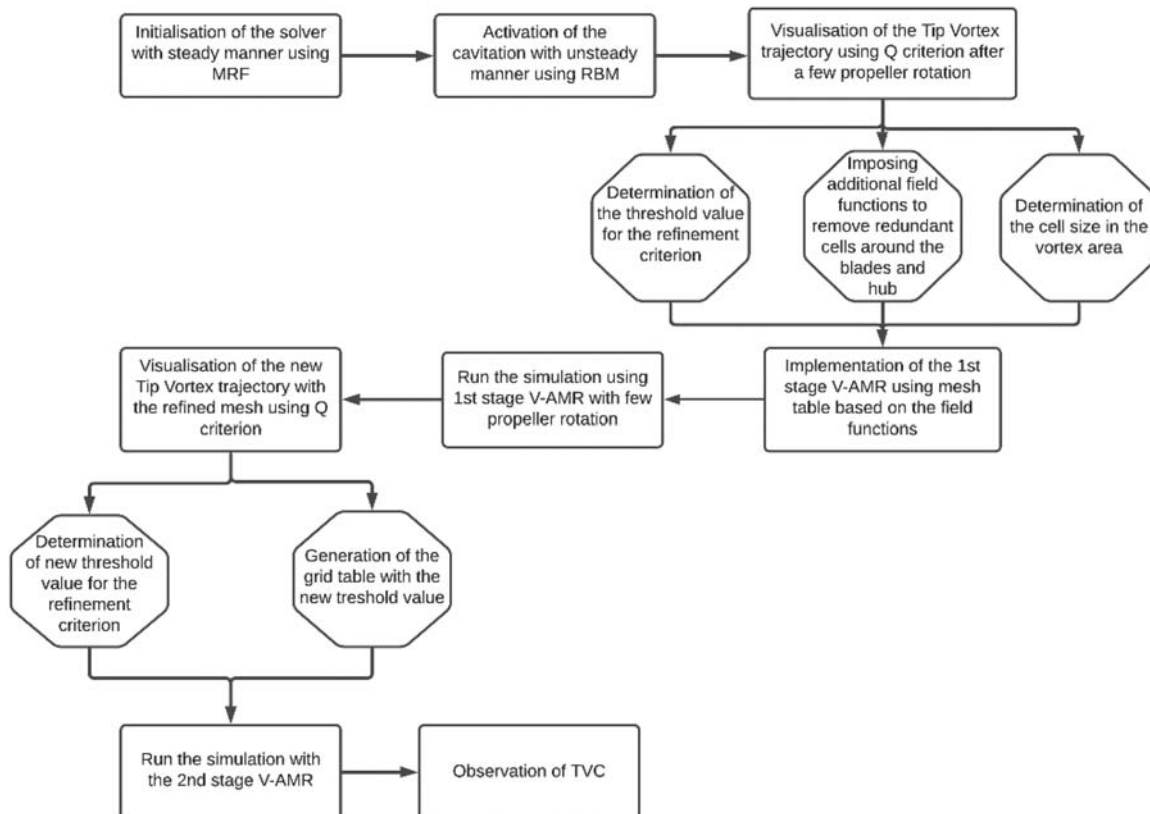


Figure 4. The flow chart of the algorithm used in V-AMR procedure.

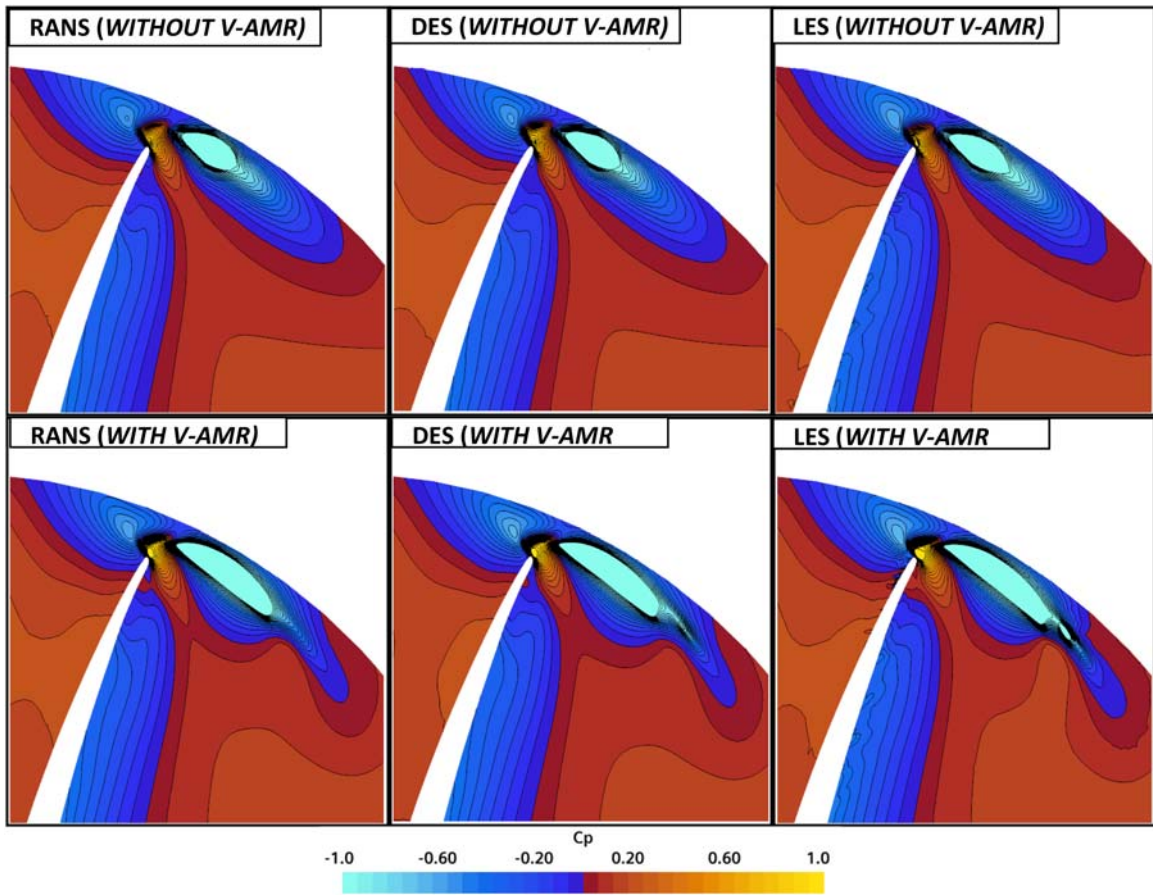


Figure 5. The change in the pressure field at  $x/D=0.05$  ( $C_p = \frac{P}{0.5\rho(nD)^2}$ ).

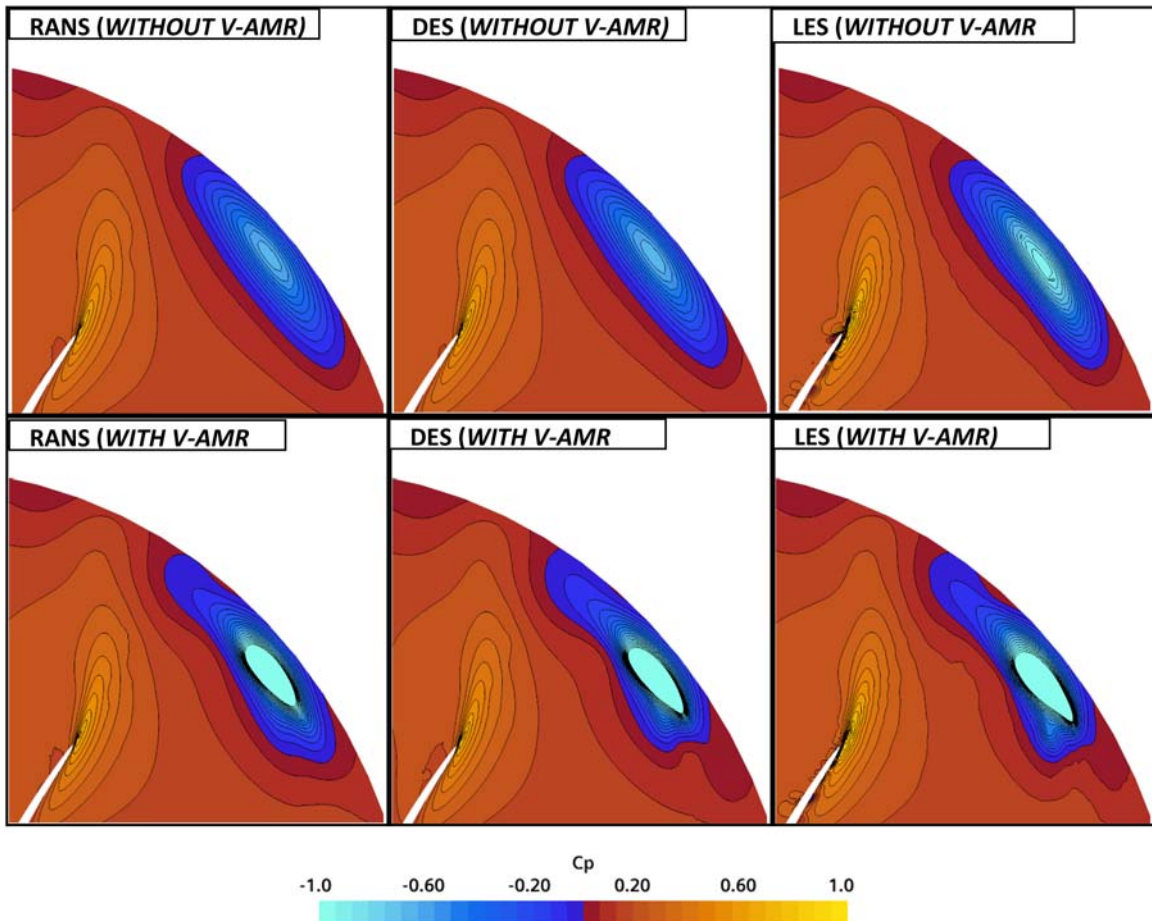
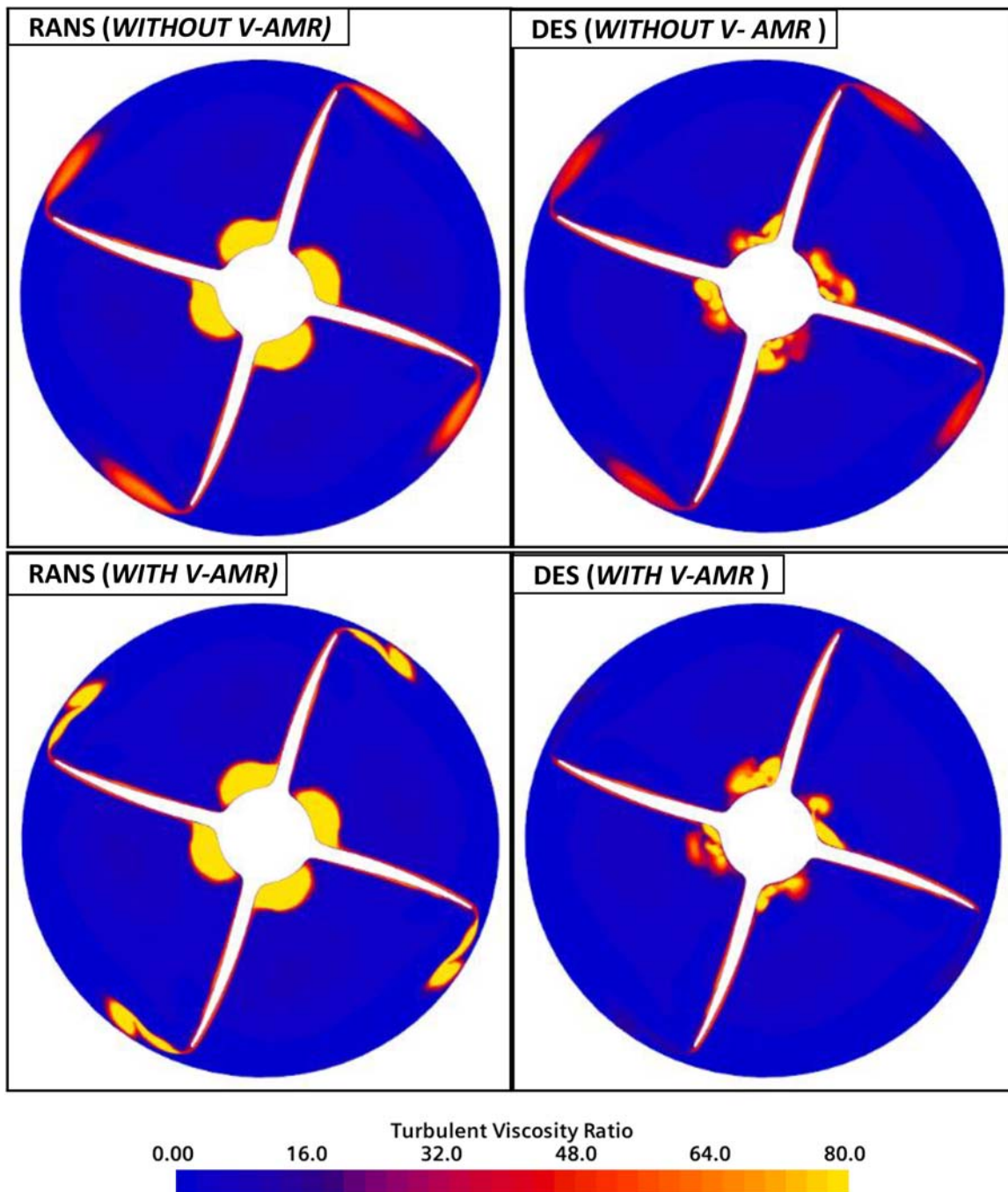


Figure 6. The change in the pressure field at  $x/D=0.1$  ( $C_p = \frac{P}{0.5\rho(nD)^2}$ ).





**Figure 7.** The change in eddy viscosity ratio at  $x/D=0.05$ .

Further comparisons were performed for the investigation of the turbulent eddy viscosity ratio patterns as shown in Figures 7 and 8 between the RANS and DES-based results as the same turbulence model was used. The turbulent eddy viscosity ratio (also known as eddy viscosity ratio) is the ratio of the turbulent viscosity ( $\mu_t$ ) and dynamic molecular viscosity ( $\mu$ ). This ratio can also be considered as an indication of the additional dissipation created by the turbulence model. As shown in Figures 7 and 8, when the V-AMR technique is applied, the RANS method presents an excessive amount of eddy viscosity compared to that predicted by the DES solver, which is expected to lead to rapid dissipation of the tip vortex in the

propeller slipstream. This is because the standard RANS solvers use the eddy viscosity concept to model the Reynolds stress tensor. This concept, which is also called the Boussinesq approximation, assumes that the anisotropic part of the Reynolds stress tensor is linearly proportional to the time-averaged strain rate tensor, and the turbulence is presumed locally isotropic (Pope 2011). Thus, the standard RANS solvers become inadequate for the accurate solution of the anisotropic turbulence inside the vortex core when compared to scale resolving simulations (i.e. DES and LES). This leads to an insufficient extension of TVC in the propeller slipstream (Wang et al. 2015). However, the V-AMR technique reduces the

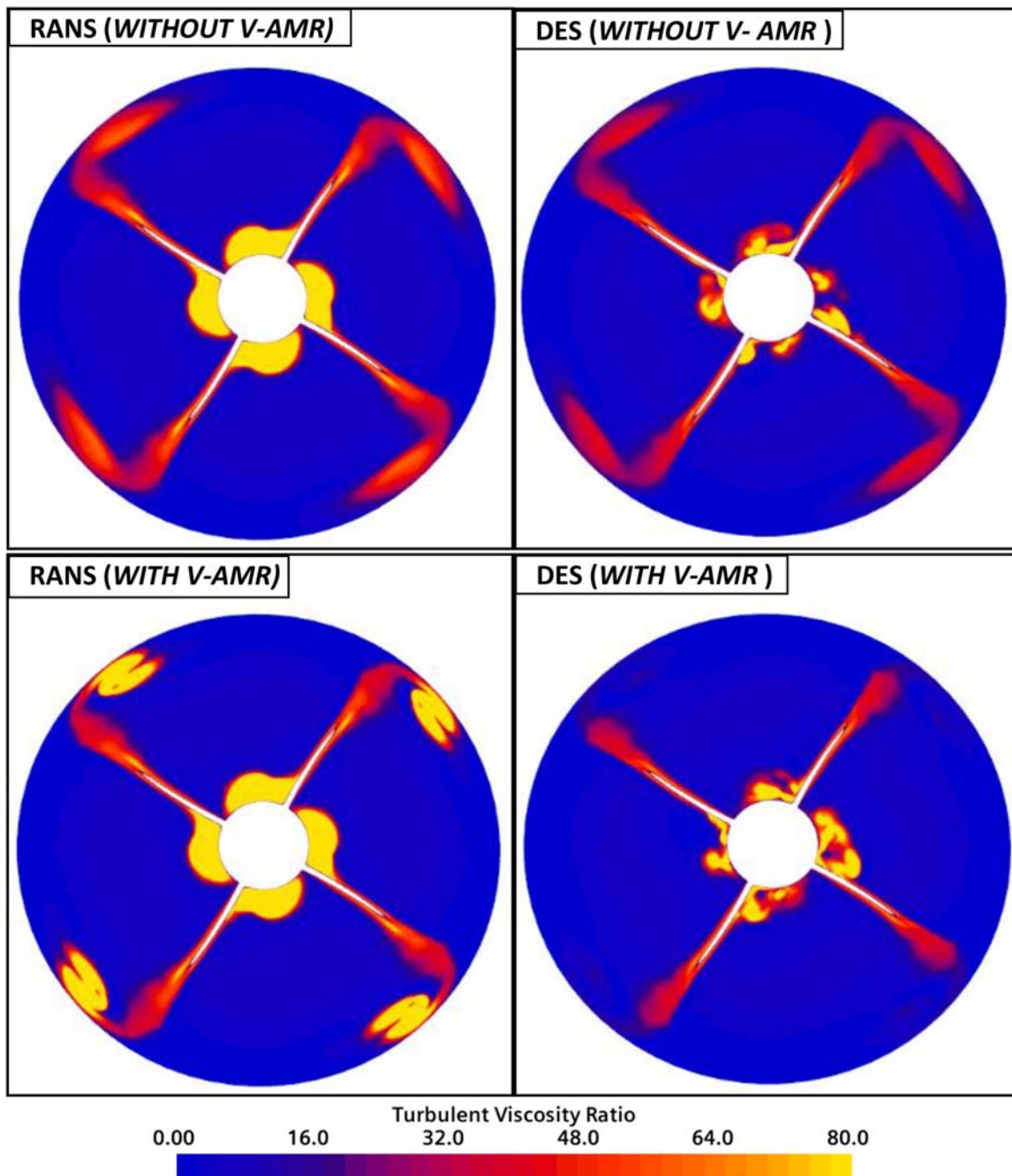


**Figure 8.** The change in eddy viscosity ratio at  $x/D=0.1$ .

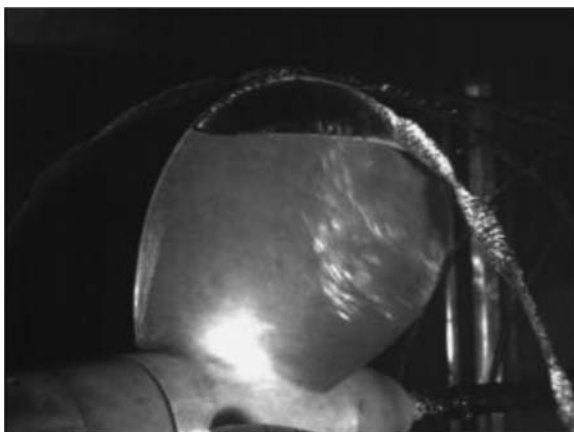


**Figure 9.** The experimental observation of cavitation pattern at  $J=0.71$  and  $\sigma = 1.763$  (Salvatore et al. 2009).

eddy viscosity ratio with the DES, which is expected to result in further extension of TVC downstream of the propeller since all turbulent scales are not modelled in the DES method compared to the RANS.

Following the investigation of the hydrodynamic field in the propeller slipstream with and without the application of the V-AMR technique, the cavitation patterns predicted by the different solvers are compared with the pattern observed in the experiment. Figure 9 shows the cavitation pattern observed in the experiment, which involved sheet, tip vortex and hub vortex cavitation at the specified operating condition.

Figure 10 compares the three cavitation types observed in the model tests with their counterparts

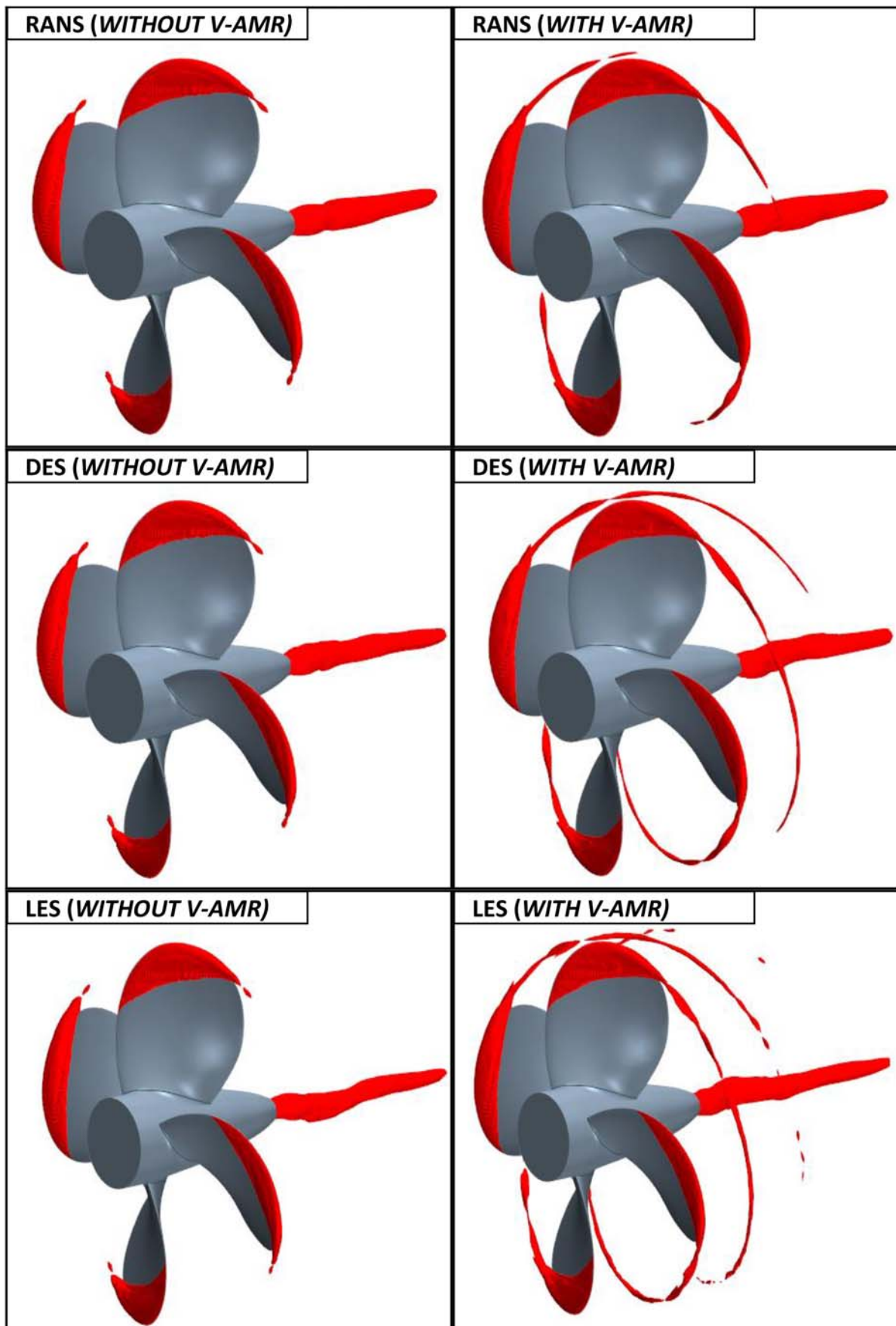


**Figure 10.** Comparison of sheet, tip and hub vortex cavitation with RANS, DES and LES ( $\alpha_v = 0.1$ ).

predicted by the RANS, DES and LES solvers with and without the application of the V-AMR technique. The red lines indicate the isosurface of  $\alpha_v=0.1$

(volume fraction of vapour). As shown in [Figure 10](#), the sheet cavitation patterns are predicted similar by all three solvers without the V-AMR technique,

**Table 3.** Comparison of hydrodynamic coefficients.

	LES			DES			RANS		
	$K_T$	$10K_Q$	$\eta_0$	$K_T$	$10K_Q$	$\eta_0$	$K_T$	$10K_Q$	$\eta_0$
WITHOUT V-AMR	0.245	0.421	0.658	0.241	0.431	0.632	0.241	0.432	0.630
WITH V-AMR	0.245	0.422	0.656	0.241	0.431	0.632	0.242	0.433	0.632
EXPERIMENT (Salvatore et al. 2009)	0.255	0.460	0.626	0.255	0.460	0.626	0.255	0.460	0.626

whereas the extension of the hub vortex cavitation is predicted differently. This is due to the superiority of the LES and DES solvers in terms of the solution of vortex structures when compared to the RANS solver. In the computations, the sheet cavitation is slightly overpredicted using different solvers in comparison with the experimental observation (see Figure 9). If one considers the three simulation results by using the V-AMR technique, an accurate representation of the tip vortex cavitation can be observed by the capture of reduced minimum pressure inside the vortex and the roll-up of the tip vortex cavitation by all three simulation methods. The application of the V-AMR technique does not change the sheet cavity pattern and hub vortex cavitation. However, large differences are observed between the RANS and DES & LES in terms of the extension of TVC downstream with applying the V-AMR technique. The excessive amount of eddy viscosity predicted inside the vortex by the RANS method results in an inadequate (shorter) extension of the TVC in the propeller slipstream compared to the DES and LES solvers. This overprediction of the turbulent viscosity around the cavity region is one of the deficiencies of the standard RANS solvers apart from the inadequate turbulence modelling. This consequently influences the accurate prediction of unsteady cavitation behaviour and development of the re-entrant jet (Goncalves et al. 2010 and Bensow 2011). Nevertheless, this needs to be further investigated in a study solely focused on this subject.

The comparison of the propeller thrust, torque and efficiency predicted by the three-simulation method against the experimentally measured values are given in Table 3. As expected, the TVC has a negligible influence on the hydrodynamic coefficients for all models. Also, the thrust and torque coefficient values were predicted similar both by the RANS and DES solvers, while these values were found to be different around 3% in comparison to those predicted by the LES solver.

## 4.2. Effects of key simulation parameters on TVC with the LES solver

In this section, the effects of the grid resolution and timestep on the prediction accuracy of the TVC were investigated. For this purpose, the LES solver was used with default cavitation parameters (i.e. water quality) since the sufficient extension of the TVC was obtained by the LES and DES solvers when compared to the RANS as indicated in previous section.

### 4.2.1. Effect of grid structure

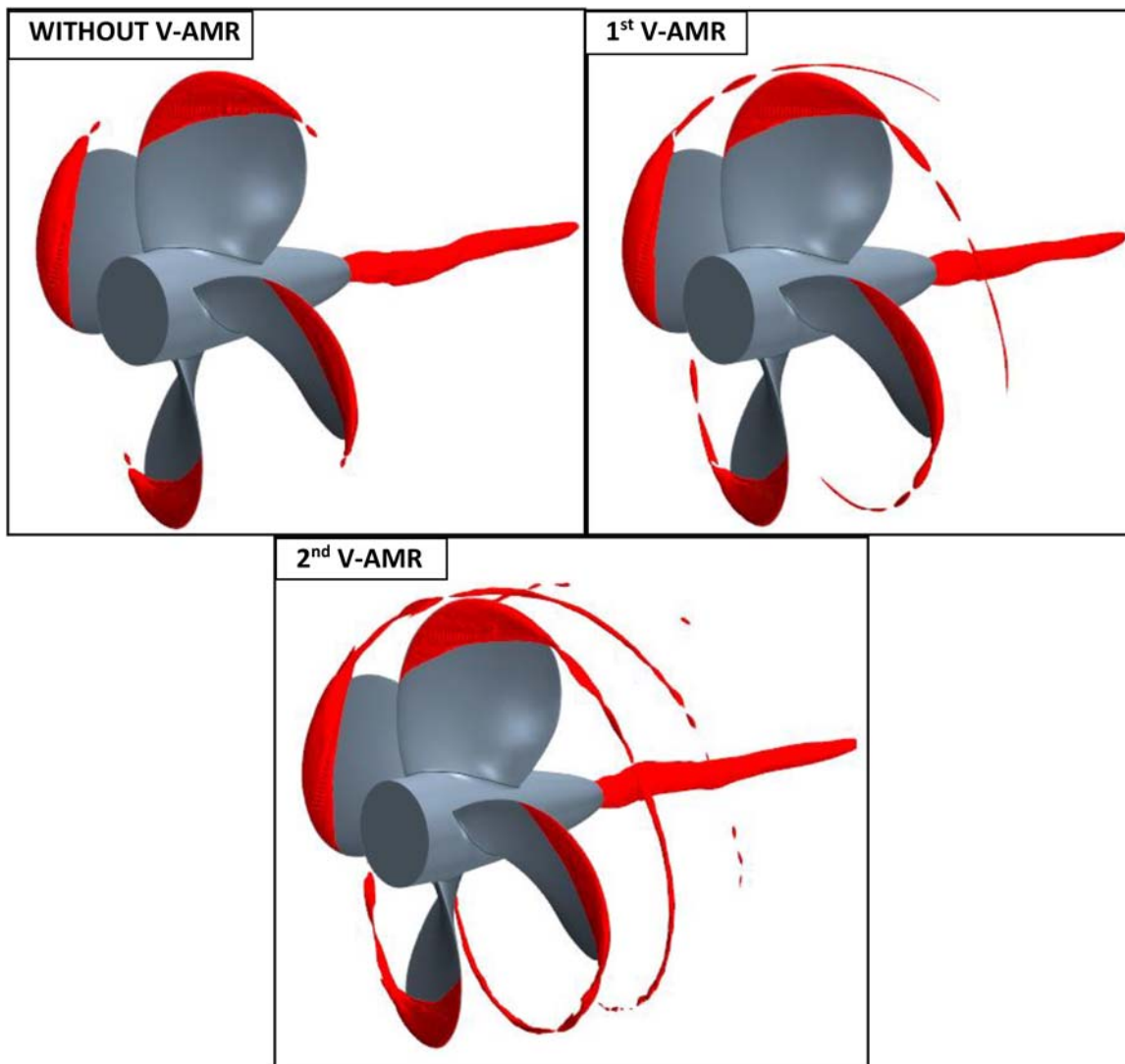
As stated in the introduction part, the accurate solution of the tip vortex is sensitive to the selection of the numerical techniques and grid resolution in the vortex region. Thus, as can be seen in Table 4, three different grid resolutions are utilised to investigate the effect of the grid resolution on the TVC extension in the propeller slipstream. It is to be noted that the time step was kept constant as  $0.5^\circ$  of the propeller rotational rate and default cavitation parameters were selected for this investigation.

Figure 11 shows the predicted TVC patterns with the application of the 1st and 2<sup>nd</sup> stages of the V-AMR technique, respectively, using a fine grid structure. As shown in Figure 11, in the 1st refinement stage, the trajectory of TVC was determined using a relatively coarse grid (i.e. 0.4 mm). Then the total extension of TVC was obtained with the application of the 2<sup>nd</sup> refinement stage of the V-AMR technique to make the solution more computationally affordable.

Figure 12 shows the change in the extensions of TVC in the propeller slipstream with an increase in the grid resolution inside the vortex. As can be seen in Figure 12, the TVC becomes more stretched downstream with an increase in the refinement level. No discernible differences could be observed between the results of the medium and fine grid structure applications. Thus, one may assume that the accurate

**Table 4.** Grid parameters for TVC extension investigation.

Grid Type	1st Refinement Cell Size (mm)	Refinement Factor (1st Refinement)	2nd Refinement Cell Size (mm)	Refinement Factor (2nd Refinement)	Total Number of Cells (Millions)
Fine w/o V-AMR	-	-	-	-	8.842.287
Fine with V-AMR	0.40	Cell Size/4	0.20	Cell Size/8	17.721.807
Medium with V-AMR	0.50	Cell Size/4	0.25	Cell Size/8	11.637.147
Coarse with V-AMR	0.60	Cell Size/4	0.30	Cell Size/8	9.083.751



**Figure 11.** Development of TVC in the propeller's slipstream with two stages of V-AMR technique using LES ( $\alpha_v = 0.1$ ).

solution of the TVC can be achieved by creating approximately 3M additional cells (i.e. medium mesh) by modelling the TVC emanating from all propeller blades. This proves the feasibility of the proposed V-AMR technique for feasible numerical applications. In addition to this, the roll-up phenomenon of the tip vortex was well captured using the different grid resolutions in comparison to that observed by the experiment, as shown in Figure 9.

In order to calculate the numerical uncertainty of the solution due to the grid spacing, the GCI (Grid Convergence Index) method was performed by following the ITTC (International Towing Tank Conference) guideline (i.e. ITTC 1999). This procedure was first proposed by Roache 1998 and is being commonly implemented in the literature by following the procedure of Celik et al. 2008. Table 5 shows the solution scalars computed by different grid resolutions at constant timestep (i.e.  $0.5^\circ$  of propeller rotational rate). Here,  $\varphi$  is the solution scalar,  $R$  is the convergence condition,  $e_a$  is the discretisation error due to the extrapolated zero grid spacing, and  $GCI_{FINE}$  is the

uncertainty level of the solution. As given in Table 5, the uncertainty level of the solution due to the grid spacing was calculated below 1% for both thrust and torques coefficients. Additionally, the convergence condition (i.e.  $R$ ) was found below than 1, which determined the solution type as monotonic convergence. It should be noted that the CFL (Courant–Friedrichs–Lewy) number was not kept constant during the uncertainty study as the GCI method is implemented using one variable. As the numerical approach is implicit, the CFL requirement is not associated with the stability of the time scheme. Nevertheless, CFL number was kept below 1, particularly in the propeller slipstream, for the accuracy of the solution for different grids.

#### 4.2.2. Influence of timestep

Apart from the grid structure and numerical modelling, another key simulation parameter is the time step for the TVC. According to the ITTC guideline (ITTC 2014), the time step is generally selected such that 0.5 and 2 degrees of propeller rotational rate.

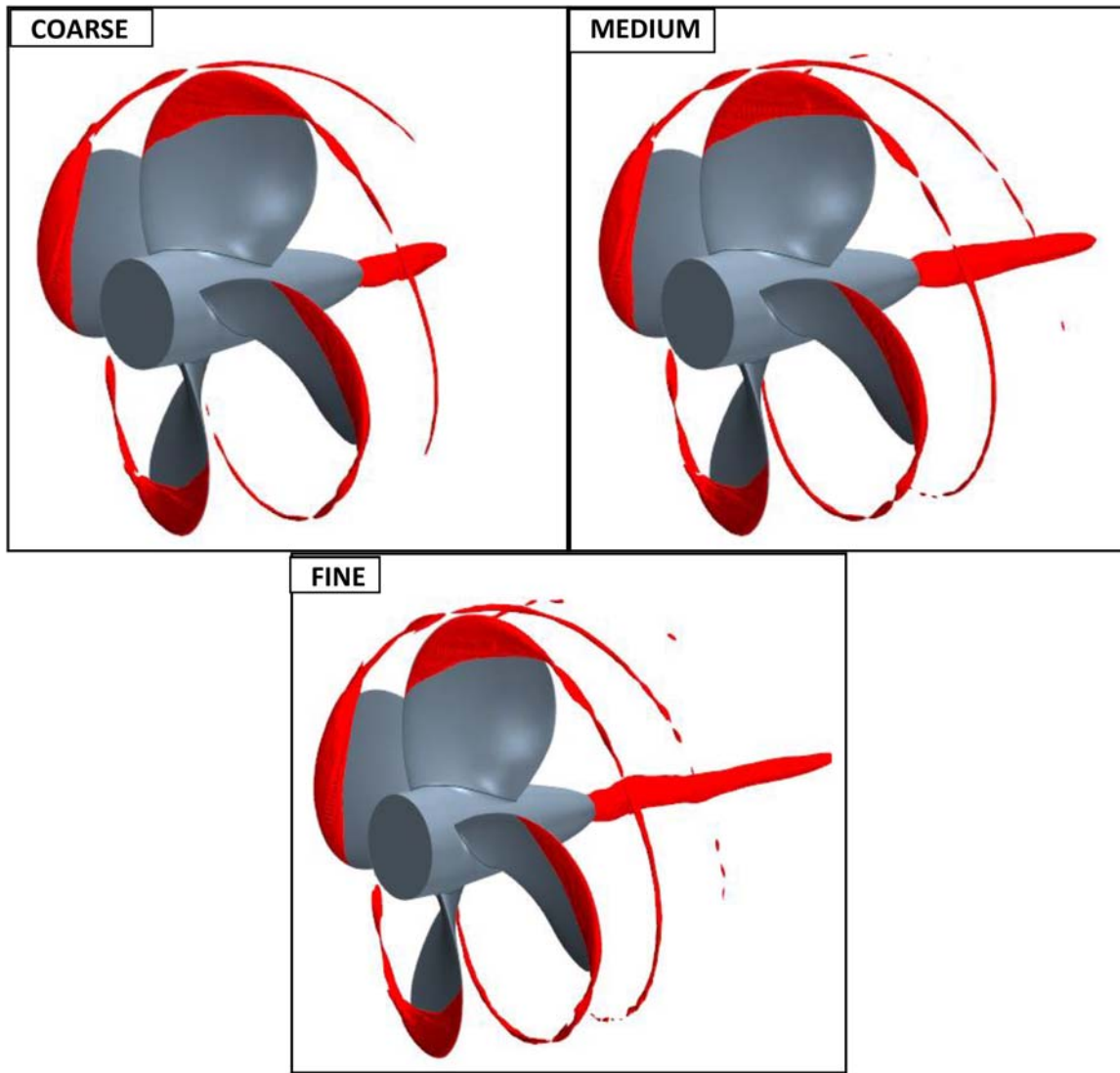


**Figure 12.** Comparison of TVC extension with different grid resolutions using LES ( $\alpha_v = 0.1$ ).

However, the recommended timestep values might be required to be decreased further according to the numerical scheme applied and algorithm for the rotating propeller and grid. Thus, the influence of the timestep on TVC was examined using the fine grid structure and four different time step values with default cavitation parameters, as shown in Table 6.

Figure 13 shows the change in the sheet, tip and hub vortex cavitation with the timestep. As shown in this figure, the shape of the sheet cavitation is found similar for the different timestep values. However, the extension of the hub and TVC was found to be sensitive to the selection of the timestep. The values

between  $0.25^\circ$  and  $0.5^\circ$  did not create considerable differences in terms of the TVC extension in the propeller slipstream. Nevertheless, slight differences were observed in the hub vortex cavitation.

The variation of the total cavity volume with the different timesteps is shown in Figure 14. As shown in this figure, the total cavity volume decreases dramatically with timestep selection as  $1^\circ$  and  $2^\circ$  of propeller rotational rate. This is mainly because of the reduction in the TVC and hub vortex cavitation.

The change in the thrust and torque values with different timesteps is given in Table 7. The uncertainty of the numerical solution due to the temporal discretisation was assessed with the GCI approach as described in Celik et al. 2008. The uncertainty level

**Table 5.** The results of the spatial convergence study.

$J=0.71, \sigma=1.763$	$K_T$	$10K_Q$
$\varphi_1$ (Fine)	0.245	0.422
$\varphi_2$ (Medium)	0.246	0.425
$\varphi_3$ (Coarse)	0.248	0.429
$R$	0.500	0.750
$e_{ext}^{21}$	2.63E-3	8.03E-3
$e_{ext}^{32}$	1.11E-2	2.11E-2
$GCI_{FINE}$ (%)	0.327	0.996

**Table 6.** The details of the selected timestep values.

Grid Type	$\Delta t$ ( $^\circ$ )	$\Delta t$ (s)
Fine	0.25	$1.959 \times 10^{-6}$
Fine	0.5	$3.858 \times 10^{-5}$
Fine	1	$7.716 \times 10^{-5}$
Fine	2	$1.543 \times 10^{-4}$

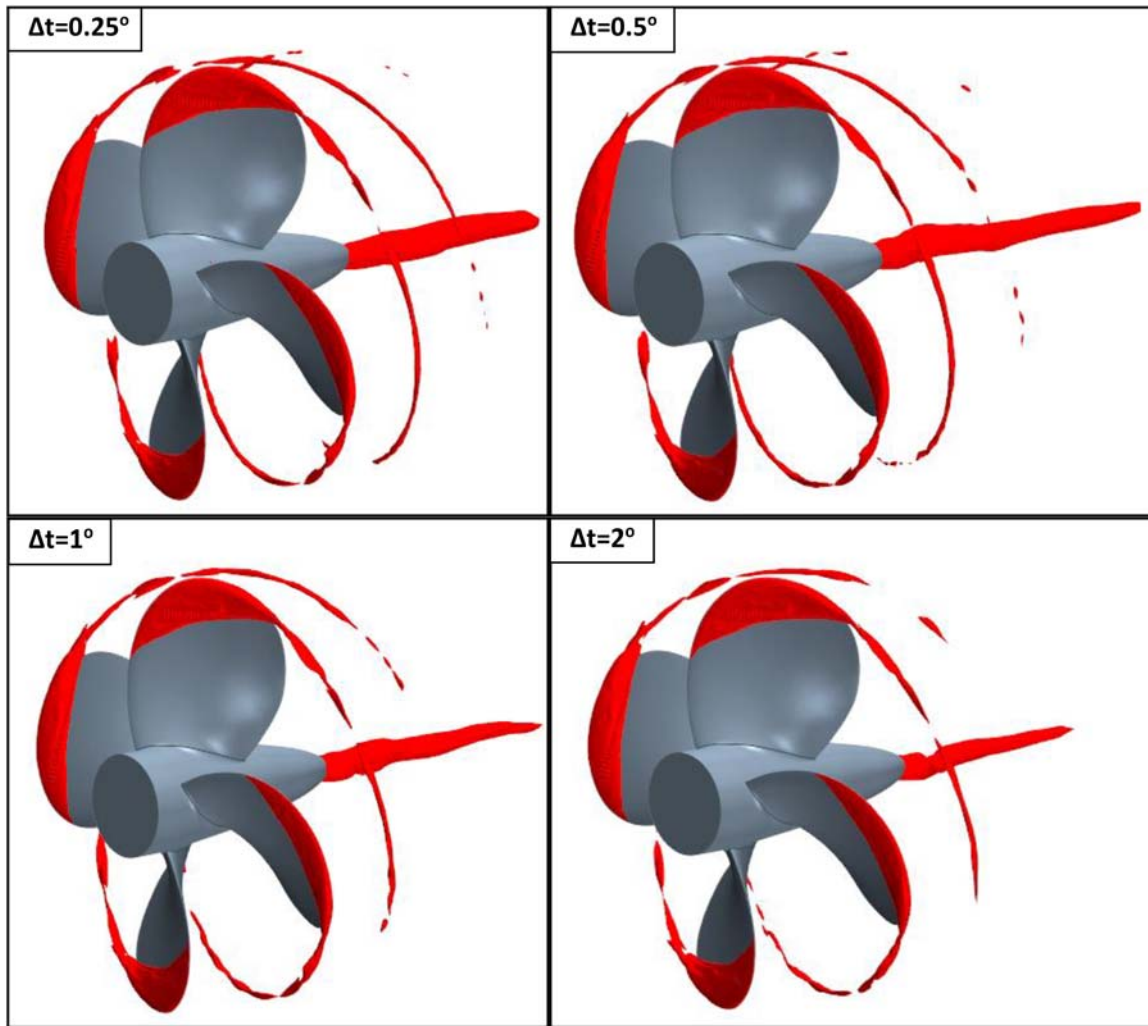


**Figure 13.** Comparison of TVC extension with different timesteps using LES ( $\alpha_v = 0.1$ ).

of the solution was found between 0.5% and 2% for thrust and torque values.

#### 4.2.3. Influence of cavitation parameters

Cavitation inception is a complex flow phenomenon, and it is strongly affected by the water quality, the

growth of the boundary layer and cavitation type (e.g. Korkut and Atlar 2012). Cavitation nuclei, which are tiny bubbles filled with water or gas or a combination of them, form the cavitation. Thus, cavitation does not incept in the water, in which there are no nuclei (i.e. filtered and degassed) (Sipilä 2012). The filtered and degassed water cavitates alternatively depending on the filtration and degassing process.

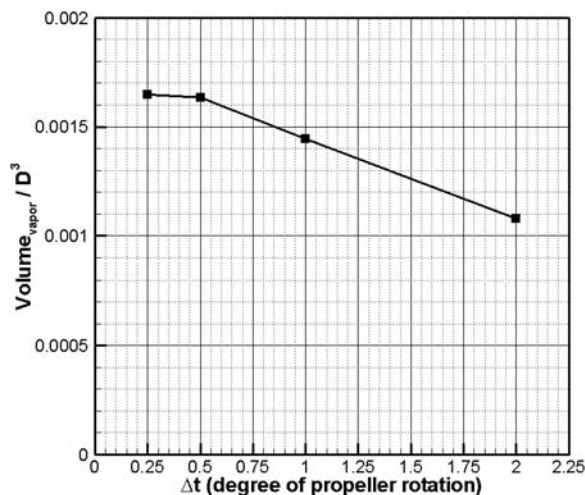


**Figure 14.** Comparison of total cavity volume using LES.

**Table 7.** The obtained hydrodynamic values and uncertainty results using a fine grid with LES.

	$K_T$	$10K_Q$
$\Delta t_1$ (°)	0.25	0.25
$\Delta t_2$ (°)	0.5	0.5
$\Delta t_3$ (°)	1	1
$\Delta t_4$ (°)	2	2
$\varphi_1$	0.246	0.423
$\varphi_2$	0.245	0.422
$\varphi_3$	0.243	0.420
$\varphi_4$	0.240	0.417
$R(\Delta t_1, \Delta t_2, \Delta t_3)$	0.500	0.500
$R(\Delta t_2, \Delta t_3, \Delta t_4)$	0.666	0.666
$e_{ext}^{21}$	4.05E-3	2.36E-3
$e_{ext}^{32}$	8.10E-3	4.72E-3
$e_{ext}^{43}$	2.41E-2	1.41E-2
$GC _{FINE}(\Delta t_1 - \Delta t_2 - \Delta t_3)$ (%)	0.508	0.296
$GC _{FINE}(\Delta t_2 - \Delta t_3 - \Delta t_4)$ (%)	2.041	1.185

**Table 8.** The selected nuclei diameter values.

Case Number	Grid Type	$\Delta t$ (°)	Analysis Type	Density (1/ $m^3$ )	Diameter (m)
1	Fine	0.5	Nuclei Diameter	$10^{12}$	$10^{-8}$
2	Fine	0.5	Nuclei Diameter	$10^{12}$	$10^{-7}$
3	Fine	0.5	Nuclei Diameter	$10^{12}$	$10^{-6}$
4	Fine	0.5	Nuclei Diameter	$10^{12}$	$10^{-5}$

In order to perform the comparison between the numerical methods and experiments for the cavitation investigations, the water quality (i.e. nuclei density and nuclei number) should be the same. However, these values are not generally measured during the measurements in the cavitation tunnels introducing some uncertainty in the inception level predicted. Hence, different commercial numerical solvers use their own default values for cavitation calculations. For instance, the FLUENT solver uses  $10^{13}$  for the nuclei density, whereas Star CCM+ suggests using  $10^{12}$  and  $10^{-6}$  for the nuclei density and diameter, respectively. Additionally, different values are used in several studies (e.g. Cazzoli et al. 2016 and Shin 2019). The selection of these values is quite scattered.

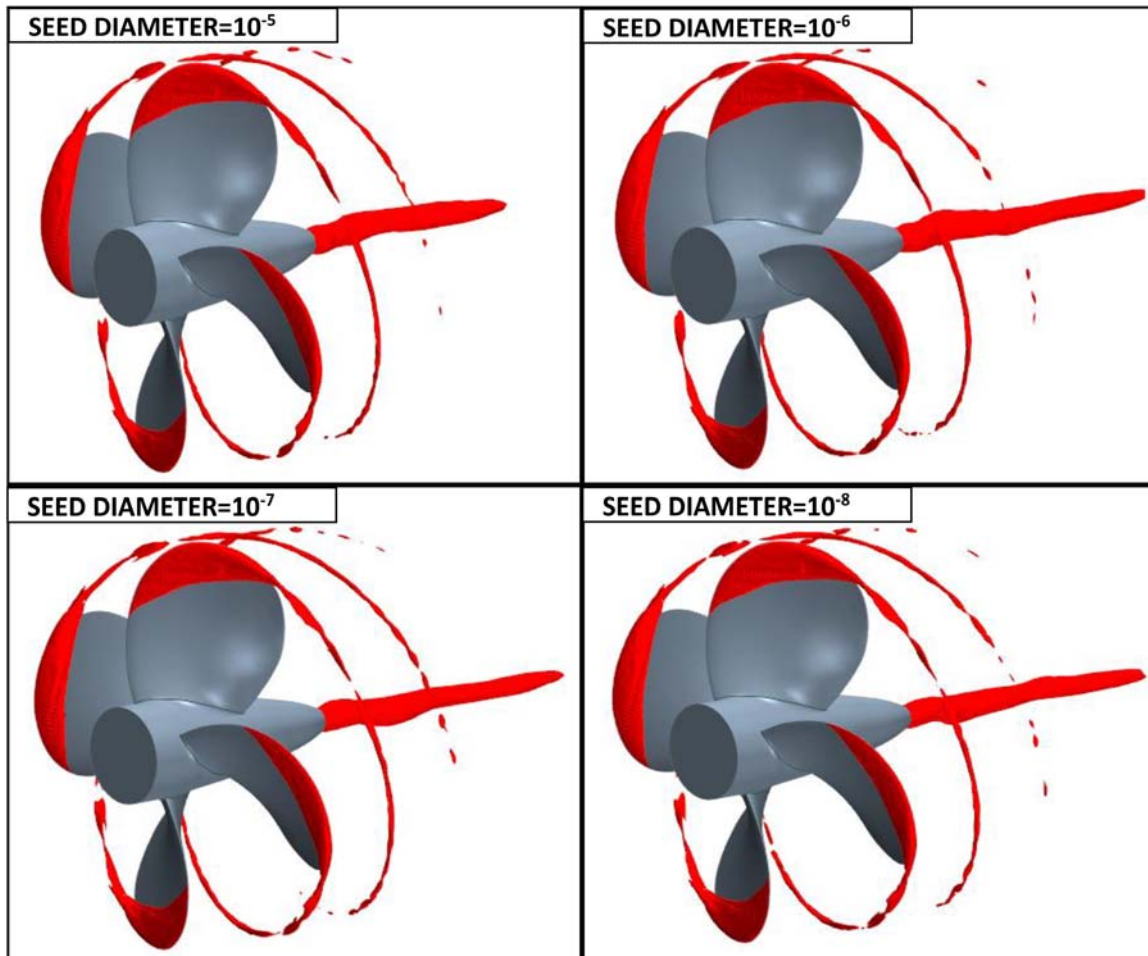
**Table 9.** The selected nuclei density values.

Case Number	Grid Type	$\Delta t$ (°)	Analysis Type	Density (1/ $m^3$ )	Diameter (m)
1	Fine	0.5	Nuclei Density	$10^{11}$	$10^{-6}$
2	Fine	0.5	Nuclei Density	$10^{12}$	$10^{-6}$
3	Fine	0.5	Nuclei Density	$10^{13}$	$10^{-6}$
4	Fine	0.5	Nuclei Density	$10^{14}$	$10^{-6}$

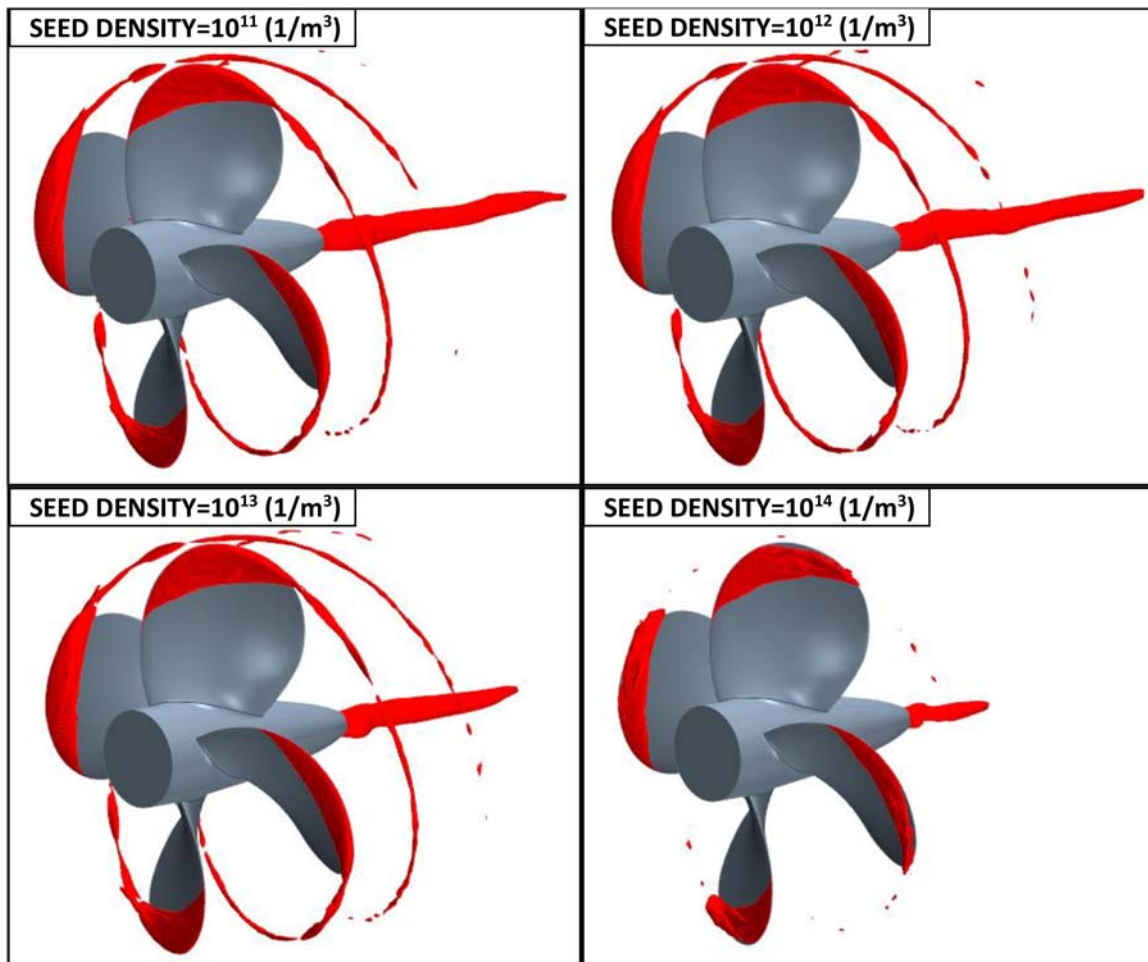
Therefore, the effects of these parameters on TVC was investigated in the following.

Table 8 shows the selected nuclei diameters for the analysis using the LES solver. Figure 15 shows the effect of the change in the nuclei diameter from  $10^{-5}$ – $10^{-8}$  at the constant nuclei density (i.e.  $10^{12}$ ) on the cavity volume and extent of the sheet, hub and tip vortex cavitation. As shown in Figure 15, the variation of the nuclei diameters has a negligible influence on the sheet and tip vortex cavitation, while slight differences can be observed in the hub vortex cavitation.

Next is the investigation of the effect of different nuclei density values on the cavitation patterns and the values used for this investigation and the selected

**Figure 15.** Variation of cavitation volume with different nuclei diameters using LES ( $\alpha_v = 0.1$ ).





**Figure 16.** Variation of cavitation volume with different nuclei densities using LES ( $\alpha_v = 0.1$ ).

values for the nuclei density are presented in Table 9. In this investigation, the nuclei diameter was kept constant at  $10^{-6}$  (i.e. default value). Figure 16 shows the resulting effect on the three cavitation patterns. As shown in Figure 16, the effect of the nuclei density is more pronounced on the tip and hub vortex cavitation as such, with the selection of higher nuclei density

values (i.e.  $10^{14}$ ), the tip and hub vortex cavitation disappear rapidly. Thus, the results suggest that higher values of nuclei density should not be selected for the tip and hub vortex cavitation investigations in the numerical studies using the Schneer Sauer Cavitation Model unless experimental values are available.

Figure 17 shows the change in the total cavitation volume with the selection of different nuclei densities and numbers. Although the effects of cavitation parameters on the hydrodynamic performance coefficients are negligible, the total cavitation volume changes significantly, particularly with the selection of higher seed densities. This analysis confirms the reliability of the default values applied in the Schneer Sauer cavitation model in the commercial solver for model scale propellers (e.g. in Star CCM+ 2019). It is recommended that these values should be explored

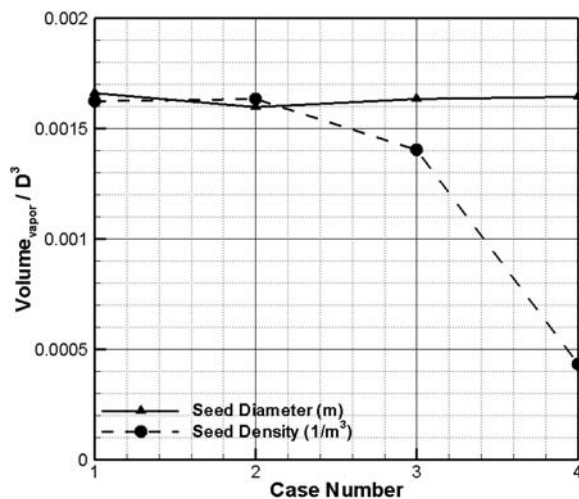


**Figure 17.** Change in total cavitation volume with different nuclei densities and diameters using LES.

**Table 10.** The details of the mesh properties in near-wall for RANS solutions.

Grid Type	Averaged $y^+$ on the blades	Prism Layer Number	Prism Layer Thickness (mm)
Fine	0.67	14	0.0013
Fine	2.7	11	0.0013
Fine	39	5	0.0013
Fine	64	4	0.0013

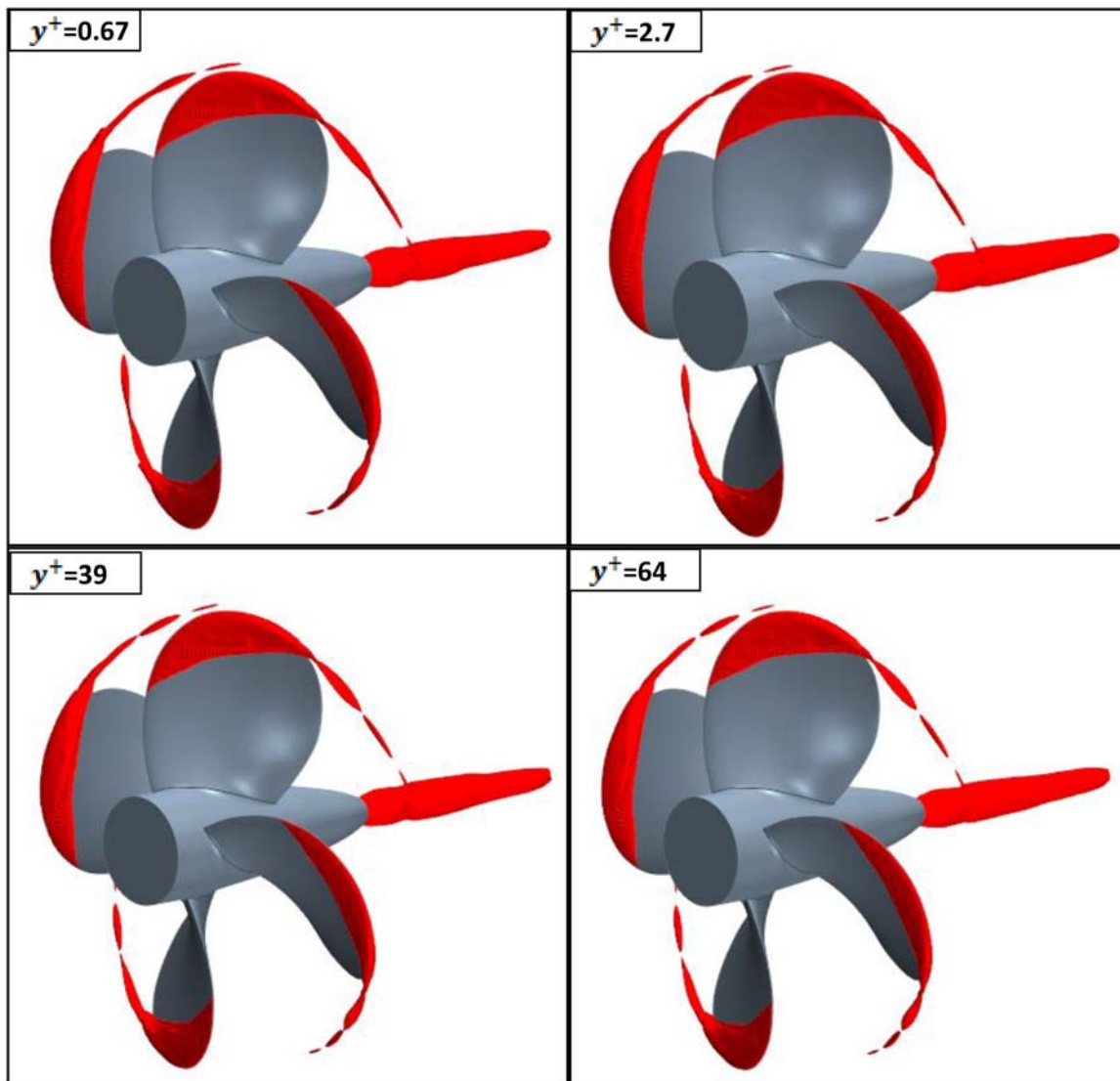


**Figure 18.** Variation of cavitation pattern with an increase in average  $y^+$  values for RANS.

with the full-scale investigations in further studies as the cavitation dynamics will be different in full-scale in comparison to the model-scale.

#### **4.3. Influence of boundary layer resolution on TVC using a standard RANS solver**

As demonstrated in the previous sections, scale resolving simulations by DES and LES are more successful in predicting the TVC compared to the predictions with the standard RANS solvers. Despite this fact, the standard RANS solvers have been generally implemented for representing cavitating flows around the propellers, particularly in the preliminary design stage. Therefore, the evolution of tip vortex was examined by changing the boundary layer resolution as the initial roll-up phenomena, and the sensitivity of the evolution of the TVC to the boundary layer solution was demonstrated in the literature (e.g. Hsiao and Chahine 2008; Gaggero et al. 2014 etc.). Here, in this section, the authors also explored such capability of

the standard RANS solvers using the subject model propeller. In this investigation, the timestep was kept constant as  $0.5^\circ$  and cavitation parameters were taken as default values (i.e. nuclei density =  $10^{12}$  and nuclei number =  $10^{-6}$ ) in the numerical calculations.

Accurate computation of the flow near-wall is important in many turbulent flow modelling. However, this requires a higher grid resolution to resolve all details in the turbulent boundary layer, especially in high Reynolds numbers. In the standard RANS solvers, this issue is commonly tackled by the implementation of the wall-function approach and considering the universal behaviour of the near-wall flows to reduce the computational cost. The wall-function approach models the flow variables near the wall by keeping the first cell of the prism layer in the log-law region (where  $30 < y^+ < 500$ ) instead of resolving (Craft et al. 2002; Versteeg and Malalasekera 2007). On the other hand, resolving the boundary layer without using the wall function increases the accuracy of the solution (Defraeye et al. 2011). To implement

the latter approach, the  $y^+$  value was kept between 0 and 5. Table 10 shows the details of the grid resolution in the boundary layer. By keeping the constant prism layer thickness and overall grid structure, only the prism layer numbers were changed from 14 to 4 with a stretching ratio of 1.5.

Figure 18 shows the change in the sheet, hub and tip vortex cavitation with different near-wall resolutions. The overall pattern of the sheet and hub vortex cavitation remained the same, both using the wall function approach and resolving the boundary layer itself. With an increase in the averaged  $y^+$ , the TVC becomes intermittent, and the extension of TVC reduces gradually. As experienced by the authors, the further increase in the average  $y^+$  values lead to the deterioration of the roll-up phenomena; thus, the considerable reduction in the extension of TVC. Due to this reason, an accurate solution of the near-wall is required to predict the TVC in using the RANS solvers.

## 5. Conclusions

This study introduced a new, alternative AMR technique (V-AMR) for the accurate realisation of TVC in a computationally efficient manner that will help wider applications of the CFD method involving TVC modelling. The technique was applied to the INSEAN E779A benchmark model propeller in open water and uniform flow conditions using three different methods and the associated commercial CFD solver. The hydrodynamic results obtained by the RANS, DES and LES solvers were compared with the experimental data with and without the TVC modelling. Additionally, the uncertainty study was conducted for grid spacing and temporal discretisation using the GCI technique. The influence of key simulation parameters on the representation of the TVC modelling was comprehensively investigated. Based on the study, it was found that:

- As the accurate solution of the TVC requires a higher grid resolution in the tip vortex regions, the proposed V-AMR technique enabled the prediction of TVC in the propeller slipstream with a minimal computational cost. The TVC was successfully observed with additional 3M cells (i.e. cell size: 0.25 mm) by modelling all propeller blades.
- As far as the different simulation techniques (i.e. RANS, DES and LES) are concerned, the overall pattern of the sheet cavitation predicted was found to be similar by using the three techniques, while that of the TVC and hub vortex cavitation differed.
- With the implementation of the V-AMR technique, the RANS solver presented an insufficient extension of the TVC in the propeller slipstream compared to

the DES and LES predictions due to the intrinsic modelling problems of the standard RANS solvers in a tip vortex flow. The more realistic TVC extension in the propeller slipstream was obtained by the DES and LES solvers.

- The influence of TVC on the global performance characteristics (i.e. thrust and torque) was found negligible. However, the accurate prediction of the TVC was found to be significantly affected by the selection of simulation techniques (i.e. RANS or DES & LES), grid resolution, timestep and water quality (i.e. nuclei density) parameters. The results suggested that the cell size inside the vortex should be between 0.2 and 0.25 mm for the realistic formation of TVC in the propeller slipstream for model scale propellers. Also, the timestep should be kept between  $0.25^\circ$  and  $1^\circ$  of propeller rotational rate in terms of the realisation of TVC. Even though the nuclei diameter has no influence on the sheet, hub and tip vortex cavitation, the hub and tip vortex cavitation are strongly dissipated with the selection of higher nuclei density values in the numerical solvers.
- The optimum cell size inside the vortex can be implemented as 0.2mm-0.25 mm for the model scale propellers when the diameter of the propeller is between 0.2 and 0.3 m. However, for the full-scale applications, the grid size inside the vortex should be enlarged with the scale ratio for the observation of TVC in the numerical solvers.
- As the standard RANS solvers are still commonly used for practical engineering applications, the representation of the TVC by using the standard RANS solvers were found to be affected by the boundary layer resolution.
- Finally, the investigations presented in this study will widen the further applications of the CFD methods involving TVC, e.g. modelling of the propeller induced URN.

This study is part of the ongoing research to predict the propeller URN in the presence of TVC. The developed V-AMR technique is currently being implemented for this purpose both in the model and full-scale URN predictions.

## Acknowledgements

The first author is sponsored by the Stone Marine Propulsion Ltd of the UK and the University of Strathclyde during his PhD study. Results were obtained using the ARCHIE-WeSt High-Performance Computer ([www.archie-west.ac.uk](http://www.archie-west.ac.uk)) based at the University of Strathclyde. The authors are grateful to CNR-INSEAN, especially Francesco Salvatore, for providing the propeller geometry.

## Disclosure statement

No potential conflict of interest was reported by the author(s).

## ORCID

Savas Sezen  <http://orcid.org/0000-0002-0852-0145>

## References

- Asnaghi A. 2018. Computational Modelling for Cavitation and Tip Vortex Flows. PhD Thesis, Department of Mechanics and Maritime Sciences, Chalmers University of Technology.
- Asnaghi A, Svennberg U, Bensow RE. 2020. Large Eddy simulations of cavitating tip vortex flows. *Ocean Eng.* 195. doi:10.1016/j.oceaneng.2019.106703.
- Bensow RE. 2011. Simulation of the unsteady cavitation on the Delft Twist11 foil using RANS, DES and LES, Second International Symposium on Marine Propulsors, SMP'11. Hamburg, Germany.
- Bensow RE, Bark G. 2010. Implicit LES predictions of the cavitating flow on a propeller. *J Fluids Eng Trans ASME.* 132:0413021–04130210. doi:10.1115/1.4001342.
- Bosschers J. 2018. Propeller tip-vortex cavitation and its broadband noise. PhD Thesis, University of Twente, Enschede, The Netherlands. <https://doi.org/10.3990/1.9789492679529>.
- Cazzoli G, Falfari S, Bianchi GM, Forte C, Catellani C. 2016. Assessment of the Cavitation Models Implemented in OpenFOAM® under DI-like Conditions, *Energy Procedia.* Elsevier Ltd, pp. 638–645. doi.org/10.1016/j.egypro.2016.11.081.
- Celik IB, Ghia U, Roache PJ, Freitas CJ, Coleman H, Raad PE. 2008. Procedure for estimation and reporting of uncertainty due to discretisation in CFD applications. *J Fluids Eng Trans ASME.* 130:0780011–0780014. doi:10.1115/1.2960953.
- Craft TJ, Gerasimov AV, Iacovides H, Launder BE. 2002. Progress in the generalisation of wall-function treatments. *Int J Heat Fluid Flow.* 23:148–160. doi:10.1016/S0142-727X(01)00143-6.
- Defraeye T, Blocken B, Koninckx E, Hespel P, Carmeliet J. 2011. Computational fluid dynamics analysis of drag and convective heat transfer of individual body segments for different cyclist positions. *J Biomech.* 44:1695–1701. doi:10.1016/j.jbiomech.2011.03.035.
- Felli M, Camussi R, Di Felice F. 2011. Mechanisms of evolution of the propeller wake in the transition and far fields. *J Fluid Mech.* 682:5–53. doi:10.1017/jfm.2011.150.
- Fine NE, Kinnas SA. 1993. A boundary element method for the analysis of the flow around 3-D cavitating hydrofoils. *J Ship Res.* 37:213–224.
- Gaggero S, Tani G, Viviani M, Conti F. 2014. A study on the numerical prediction of propellers cavitating tip vortex. *Ocean Eng.* 92:137–161. doi:10.1016/j.oceaneng.2014.09.042.
- Goncalves E, Decaix J, Patella RF. 2010. Unsteady simulation of cavitating flows in Venturi, *Journal of Hydrodynamics.* China Ocean Press, pp. 753–758. doi:10.1016/S1001-6058(10)60026-1.
- Gosda R, Berger S, Abdel-Maksoud M. 2018. Investigation of Reynolds number scale effects on propeller tip vortex cavitation and propeller-induced hull pressure fluctuations. 10th International Symposium on Cavitation (CAV2018), Baltimore, MD.
- Guilmineau E, Deng GB, Leroyer A, Queutey P, Visonneau M, Wackers J. 2015. Influence of the Turbulence Closures for the Wake Prediction of a Marine Propeller, Fourth International Symposium on Marine Propulsors, SMP'15. Austin, Texas, USA.
- Hirt CW, Nichols BD. 1981. Volume of fluid (VOF) method for the dynamics of free boundaries. *J Comput Phys.* 39:201–225. doi:10.1016/0021-9991(81)90145-5.
- Hsiao C-T, Chahine G. 2008. Scaling of Tip Vortex Cavitation Inception for a Marine Open Propeller, 27th Symposium on Naval Hydrodynamics. Seoul, Korea.
- Hunt JCR, Wray AA, Moin P. 1988. Eddies, streams, and convergence zones in turbulent flows. *Cent. Turbul. Res. Proc. Summer Program.* 193–208. <https://doi.org/CTR-S88>.
- ITTC. 1999. ITTC-Recommended Procedures and Guidelines ITTC Quality System Manual Recommended Procedures and Guidelines Procedure CFD User's Guide 7.5-0301-0.4.
- ITTC. 2014. ITTC-Recommended Procedures and Guidelines, Practical Guidelines for Ship Self-Propulsion CFD 7.5-03 -03-01.
- Konno A, Wakabayashi K, Yamaguchi H, Maeda M, Ishii N, Soejima S, Kimura K. 2002. On the mechanism of the bursting phenomena of propeller tip vortex cavitation. *J Mar Sci Technol.* 6:181–192. doi:10.1007/s007730200006.
- Korkut E, Atlar M. 2012. An experimental investigation of the effect of foul release coating application on performance, noise and cavitation characteristics of marine propellers. *Ocean Eng.* 41:1–12. doi:10.1016/j.oceaneng.2011.12.012.
- Krasilnikov V. 2019. CFD modelling of hydro-acoustic performance of marine propellers: Predicting propeller cavitation, Numerical Towing Tank Symposium, NuTTS'2019. Tomar, Portugal.
- Kuiper G. 1981. Cavitation inception on ship propeller models. PhD Thesis, Delft University of Technology.
- Lee H, Kinnas SA. 2004. Application of a boundary element method in the prediction of unsteady blade sheet and developed tip vortex cavitation on marine propellers. *J Ship Res.* 48:15–30.
- Lloyd T, Vaz G, Rijpkema D, Reverberi A. 2017. Computational fluid dynamics prediction of marine propeller cavitation including solution verification. Fifth International Symposium on Marine Propulsors, SMP'17, Espoo, Finland.
- Muscari R, Di Mascio A, Verzicco R. 2013. Modeling of vortex dynamics in the wake of a marine propeller. *Comput Fluids.* 73:65–79. doi:10.1016/j.compfluid.2012.12.003.
- Pope SB. 2011. *Turbulent flows*, Cambridge University Press. Hamburg, Germany: Cambridge University Press.
- Qiu W, Peng H, Ni S, Liu L, Mintu S, Hally D, Hsiao CT. 2013. RANS computation of propeller tip vortex flow. *Int J Offshore Polar Eng.* 23:73–79.
- Queutey P, Deng G, Wackers J, Guilmineau E, Leroyer A, Visonneau M. 2012. Sliding grids and adaptive grid refinement for RANS simulation of ship-propeller interaction. *Ship. Technol. Res.* 59:44–57. doi:10.1179/str.2012.59.2.004.
- Roache PJ. 1998. Verification of codes and calculations. *AIAA J.* 36:696–702. doi:10.2514/2.457.
- Salvatore F, Streckwall H, Van Terwisga T. 2009. Propeller Cavitation Modelling by CFD-Results from the VIRTUE 2008 Rome Workshop, First International Symposium on Marine Propulsors, SMP'09. Trondheim, Norway.
- Schnerr GH, Sauer J. 2001. Physical and Numerical Modeling of Unsteady Cavitation Dynamics, 4<sup>th</sup> International Conference on Multiphase Flow, ICMF-2001. New Orleans, USA.
- Shin KW. 2019. CFD Analysis of Ship Propeller Thrust Breakdown, Sixth International Symposium on Marine Propulsors, SMP'19. Rome, Italy.

- Shin KW, Andersen P. 2018. CFD Analysis of Propeller Tip Vortex Cavitation in Ship Wake Fields, 10th International Symposium on Cavitation, CAV2018. Baltimore, Maryland, USA.
- Sipilä T. 2012. RANS analyses of cavitating propeller flows. PhD Thesis, Aalto University School of Engineering.
- Spalart PR, Deck S, Shur ML, Squires KD, Strelets MK, Travin A. 2006. A new version of detached-eddy simulation, resistant to ambiguous grid densities. *Theor. Comput. Fluid Dyn.* 20:181–195. doi:10.1007/s00162-006-0015-0.
- Star CCM+ 14.06. 2019. User Guide, Siemens, User Guide.
- Usta O, Korkut E. 2018. A study for cavitating flow analysis using DES model. *Ocean Eng.* 160:397–411. doi:10.1016/j.oceaneng.2018.04.064.
- Versteeg HK, Malalasekera W. 2007. *An Introduction to Computational Fluid Dynamics: The Finite Volume Method* - Henk Kaarle Versteeg, Weeratunge Malalasekera, 2nd Editon. ed. Pearson.
- Viitanen V, Siikonen T. 2017. Numerical simulation of cavitating marine propeller flows. 9th National Conference on Computational Mechanics, MekIT-17.
- Wackers J, Queutey P, Visonneau M. 2010. Adaptive Grid Refinement Applied to RANS Ship Flow Computation. 28th Symposium on Naval Hydrodynamics, Pasadena, California, 12-17 September.
- Wang B, Liu Z, Peng X, Liu D. 2015. Simulations of tip vortex cavitation flows with nonlinear k- $\epsilon$  model, *Journal of Physics: Conference Series*. Institute of Physics Publishing, p. 012187.
- Windt J, Bosschers J. 2015. Influence of local and adaptive mesh refinement on the tip vortex characteristics of a wing and propeller, *MARINE 2015 - Computational Methods in Marine Engineering VI*. pp. 862–873.
- Yilmaz N, Atlar M, Khorasanchi M. 2019. An improved Mesh Adaption and Refinement approach to Cavitation Simulation (MARCS) of propellers. *Ocean Eng.* 171:139–150.
- Yvin C, Muller P. 2016. Tip Vortex Cavitation Inception Without a Cavitation Model, 19th Numerical Towing Tank Symposium (NuTTS 2016), Nantes, France.
- Zhu G. 2019. A numerical investigation of a winglet-propeller using an LES model. *J Mar Sci Eng.* 7:333. doi:10.3390/jmse7100333.